



**Politecnico
di Torino**

POLITECNICO DI TORINO

Master's Degree in ELECTRONIC ENGINEERING

A.Y. 2021/2022

Graduation session April 2022

GENERATION OF HIGH SPECTRAL PURITY MICROWAVE WITH PHOTONIC TECHNIQUES AND LOW NOISE SYNTHESIS CHAIN FOR PRIMARY FREQUENCY STANDARDS

Supervisors:

Prof. Giovanni A. COSTANZO

Dr. Cecilia CLIVATI

Candidate:

Vincenzo PICCINNI

*To my mum, my father and my sister:
I put a lot of effort,
they invested their lives in it*

Acknowledgements

I would like to thank my supervisor prof. Giovanni Costanzo and my co-supervisor Dr. Cecilia Clivati both for the opportunity that was given to me and because they constantly followed me dedicating time and attention to me.

Thanks to Eng. Calosso for his indispensable advice and knowledge transmitted during the initial part of my thesis and on topics such as phase noise and digital synthesizers (DDS) of which he is one of the leading international experts.

I would like to thank Dr. Filippo Levi and Dr. Michele Gozzelino for assisting me during the stability measurements on the Italian frequency standard with cold Cs atoms. Thanks to Dr. Elio Bertacco for providing me with technical support.

Thanks in general to INRiM and Quantum Metrology and Nanotechnology division for welcoming me and for providing me with the necessary equipment to complete this experience. Satisfaction and gratitude is what I would like to emphasize at the end of this work.

Thanks to my family for always motivating me throughout my academic career, I dedicate my goal to them.

Table of Contents

List of Figures	IX
Acronyms	XII
1 Theoretical definitions	3
1.1 PSD: Power Spectral Density	3
1.2 Basics of noise	4
1.2.1 Phase and Frequency Noise	4
1.2.2 Thermal (Johnson) noise	5
1.2.3 Shot noise	6
1.2.4 Flicker noise	6
1.2.5 Noise Figure	7
1.2.6 Spurs	7
1.2.7 Residual Noise analysis	7
1.3 Allan Deviation	9
2 Caesium Fountain and Optical Comb	11
2.1 Caesium Fountain	11
2.1.1 Atomic Clock physical principle	11
2.1.2 Dick effect and Noise budget	14
2.1.3 Microwave synthesis chain	14

2.2	Optical Frequency Comb	16
3	Chains Design: 10 GHz to 9.192 GHz	20
3.1	Characterization of Phase Noise Analyzer	21
3.2	First Chain	22
3.2.1	Characterization of Divider by 4	23
3.2.2	Characterization of the DDS	24
3.2.3	Characterization of Amplifiers	25
3.2.4	Characterization of Single-Sideband Mixer	28
3.2.5	Noise of the complete chain	29
3.3	Second Chain	33
3.3.1	Characterization of Divider by 25	33
3.3.2	Characterization of Multiplier by 2	34
3.3.3	Noise of complete chain	36
3.4	Chains comparison	39
4	Analysis of long-term effects	42
4.1	Long-term measurement set-up	42
4.2	Stability comparison between new and old chain	44
4.3	Temperature sensitivity	45
5	Stability measurements with the new synthesis chain	50
5.1	Microwave synthesis with the Optical Comb	50
5.2	Interrogating Cs atoms in the fountain clock with the optically-synthesized microwave	53
5.2.1	Ramsey scans	53
5.2.2	Stability measurement	53
	Datasheet	56

List of Figures

1.1	General scheme of a phase noise measurement. This measurement scheme will be used for almost all phase noise measurements	8
1.2	5125A Microsemi Phase Noise Analyzer blocks scheme. Source: [5125 Datasheet]	9
2.1	General scheme of an atomic clock. E1 is the fundamental state, E2 is the excited state	12
2.2	A cutaway drawing of IT-CsF2 showing the 1,1,1 molasses region, the detection region, and the cryogenic microwave interrogation region. The overall height is about 2.5 m. Source: ["NIST F1 AND F2" [11]] . . .	12
2.3	Fountain clock description. Source: [Atomic fountain clocks - R. Wynands, S. Weyers - https://iopscience.iop.org/article/10.1088/0026-1394/42/3/S08]	13
2.4	Scheme of the synthesis chain used in ITCsF2. Source:[Accuracy evaluation of ITCsF2: a Nitrogen cooled Cesium Fountain - Levi, Calonico, Calosso, Godone, Micalizio, Costanzo]	15
2.5	Menlo System 10GHz/100MHz RF generator schematic. The schematic shows the path of the signal deriving from the Optical Frequency Comb in red, it is an optical fiber connection; the electrical RF connections are shown in blue; in green the power supply connections.	17
2.6	Menlo System 10GHz/100MHz RF generator photo	18
3.1	Phase noise of Phase Noise Test with an input signal of 13 dBm split into two signals. These two signals are sent as input and reference for the phasometer.	22
3.2	Complete first chain: from 10 GHz to 9.192 GHz	22

3.3	Phase Noise of Divider by 4. In blue: input signal at 800 MHz and an output signal at 200 MHz; in black: input signal at 1.6 GHz and an output signal at 400 MHz	24
3.4	Phase Noise of DDS. In blue: the input signal is at 2.5 GHz, the output at 200MHz; in black: the input signal is at 2.5 GHz, the output at 400 MHz	25
3.5	Block Chain for amplifiers phase noise measurements	26
3.6	Phase Noise of Amplifier ZKL-1R5+: in blue at 100 MHz, in black at 400 MHz	27
3.7	Phase Noise of Amplifier WNA-220: in blue at 200 MHz, in black at 400 MHz	27
3.8	8 MHz to IF1 channel	28
3.9	8 MHz to IF2 channel	28
3.10	Complete first chain: from 10 GHz to 9.192 GHz	29
3.11	Residual noise of the first chain, generating a 9.192 GHz microwave from a 10 GHz signal. 3 dB have been removed from the raw measurement to take into account that two identical chains were compared	30
3.12	Harmonics of chain 1 with a SPAN of 500 Hz	31
3.13	Spurs of chain 1 with a SPAN of 200 kHz	32
3.14	Complete second chain: from 10 GHz to 9.192 GHz	33
3.15	Phase noise of divider by 25 RF-BAY FBS-25-14 at 10 GHz	34
3.16	Configuration for multiplier by 2 phase noise measurement	35
3.17	Phase noise of multiplier by 2 with 100 and 200 MHz input signals . . .	35
3.18	Complete second chain: from 10 GHz to 9.192 GHz	36
3.19	Phase noise of complete second chain: from 10 GHz to 9.192 GHz. 3 dB have been removed from the raw measurement to take into account that two identical chains were compared	37
3.20	Harmonics of chain 2 with a SPAN of 200 kHz	38
3.21	Harmonics of chain 2 with a SPAN of 500 Hz	38
3.22	Comparison between phase noise of complete two chains and residual noise of the DDS. 3 dB have been removed from the measurement for each curve to take into account that two identical chains were compared	39

3.23	Comparison between Allan Deviation curves of two chains	40
4.1	Block diagram of the chain as mounted for preliminar noise test (left), and in the present configuration (right)	42
4.2	Chain 2 mounted inside the aluminum box.	43
4.3	Frequency stability of previous chain vs new chain	44
4.4	Measurement setup used to determine the temperature sensitivity	45
4.5	Temperature Sensitivity measurement	46
4.6	Temperature variation in the Measurement Lab	48
4.7	Allan Deviation curve of Temperature variation in the Measurement Lab	48
5.1	Measurement scheme with Optical Frequency Comb	51
5.2	Spectrum of complete chain with Optical Comb signal as input	51
5.3	PSD of Yb laser, Comb and the conversion unit and synthesis chain . .	52
5.4	Ramsey fringes	53
5.5	Frequency stability of fountain with old chain vs new chain	54

Acronyms

DDS Direct Digital Synthesizer

PSD power spectral density

FFT Fast Fourier Transform

DFT Discrete Fourier Transform

PM Phase Modulation

FM Frequency Modulation

SNR Signal to Noise Ratio

DUT Device Under Test

ADC Analog to Digital Converter

LO Local Oscillator

NIST National Institute of Standard and Technology

LIVS Low Velocity Intense-Source

PLL phase locked loop

DRO Dielectric Resonator Oscillator

OFC Optical Frequency Comb

FOFC Fiber-based Optical Frequency Comb

MLL mode locked laser

SI International System

SSB single side-band

RBW Resolution Bandwidth

NTC Negative Temperature Coefficient

NMR Nuclear Magnetic Resonance

MOT Magneto-Optical Trap

OM Optical Molasses

CSO Cryogenic-Sapphire Oscillator

VCO Voltage Control Oscillator

RF Radio Frequency

BVA Besson Vieillissement Amélioré

Introduction

The objective of the thesis is the design of a low-noise synthesis chain that generates a signal at the frequency of 9.192631770 GHz starting from a 10 GHz signal coming from an optical comb for the interrogation of a primary frequency standard. The chain must have a lower noise than the one which is currently used.

All the work was carried out at INRiM in Turin in the Quantum Metrology and Nanotechnology division, in the "atomic frequency standards" team. Within the division, the primary national frequency standard is maintained, a Caesium fountain atomic clock which realizes the "second", unit of measurement of time in the International System. The "second" is currently defined as the *"time interval which contains 9192631770 periods of the radiation corresponding to the transition between the two hyperfine levels of the ground state of the 133 caesium atom"*. This definition is physically realized by primary atomic clocks, in which a low-noise microwave oscillator at 9193631770 Hz is kept on resonance with the Cs atomic transitions. INRiM primary clock IT-CsF2 realizes the second with a relative uncertainty of $2 \cdot 10^{-16}$, and is one of the most accurate in the world.

Photonic techniques, based on an ultra-stable laser and an optical frequency comb (OFC), allow generating a microwave with a higher spectral purity compared to classical microwave techniques based on the frequency multiplication of a low-noise RF quartz oscillator. In this perspective, the objective of my thesis is to produce the signal to interrogate the Caesium atoms at 9192631770 Hz starting from a 10 GHz signal obtained with an optical comb with a higher spectral purity between 1 Hz and 10 Hz than the synthesis chain currently used. The frequency range indicated above is relevant because the noise produced in this spectral window directly reflects on the Cs clock stability via the so-called "Dick Effect", which arises during the Cs atom interrogation and depends on the specific interrogation method is used.

During my activity, two design ideas for the low-noise synthesis chain were chosen and compared: a first chain including both analog and digital components and a second chain using exclusively analog components.

The two chains were assembled and compared in terms of phase noise and stability. The best performing chain was characterized as a function of the temperature sensitivity and used to interrogate the Caesium atoms in IT-CsF2. Finally, compared the clock performances using the previous and the new chain.

Thesis overview. The thesis is divided into five chapters: the first introduces the theoretical aspects of the measurements; the second describes the framework in which this project is carried on and introduces in particular the Caesium fountain and the optical frequency comb; the third chapter describes the characterization of the two chains and the comparison between them; the fourth chapter focuses on the analysis of long-term instability and the fifth describes the integration of the chain into the opto-electric system used to interrogate the atoms of the fountain; the conclusions chapter, at the end, collects all the results obtained.

The chance of working with a primary national frequency standard was certainly the most fascinating and stimulating thing in the development of the entire project. Thanks also to the achievement of the target performances of the chain, it is possible to say that it was a satisfying experience.

Chapter 1

Theoretical definitions

The study, the characterization of the chains and the purpose of the whole project have as their basic notions the common interest in the treatment of noise for the comparison and the definition of a high-performance solution. To discuss all these topics it is necessary to introduce some theoretical notions that will be further detailed in the rest of the thesis.

1.1 PSD: Power Spectral Density

The main objective of the thesis concerns the analysis of the phase noise in oscillators which is quantified in terms of Power Spectral Density (PSD). The PSD $S(f)$ describes the distribution of the signal power into its frequency components. A PSD is typically used to characterize broadband random signals and noise processes: in that situation the PSD of the random phase $\theta(t)$, denoted with $S_{\theta}(f)$, has the dimension of rad^2/Hz . [1][2]

The properties of the PSD are regulated by the Parseval theorem, which states that the power of a generic signal $x(t)$ calculated in the time domain and in the frequency domain is the same:

$$P = \lim_{T \rightarrow \infty} \frac{1}{T} \int_0^T |x(t)|^2 dt = \int_0^{\infty} S_x(f) df \quad (1.1)$$

where T is the observation time; a second property states that the power of the $x(t)$ after band-pass filtering is calculated by integrating the PSD over the filter bandwidth. The Power P of the filtered signal could be written as:

$$P = \int_a^b S_x(f)df = \int_a^b S_x(f) \cdot |H(f)|^2 df \quad (1.2)$$

where a and b are the band limits and $|H(f)|^2$ is the transfer function of the filter.

The PSD is calculated using the Fast Fourier Transform (FFT) algorithm. The FFT is one of the most important algorithms in signal processing and data analysis. The algorithm computes the Discrete Fourier transform (DFT) of a sequence, or its inverse, enabling its frequency-domain analysis. To calculate the DFT, the continuous signal is first converted into discrete values, sampling and truncating appropriately. Then, assuming $X(f)$ for the DFT, the subscript T for the truncation over the measurement time of duration T and f_s for the sampling frequency, the computed PSD is obtained from the DFT

$$S_x(f) = \frac{2}{T}|X_T(f)|^2 \quad \text{for } 0 < f < f_s/2 \quad (1.3)$$

The factor 2 is given by physical requirement of energy conservation. The energy of $X_T(f)$ is equally split between negative frequencies and positive frequencies with the energy associated to the negative frequencies of $X_T(f)$ folded to the positive frequencies in $S_x(f)$.

Finally, it is a common practice to improve the confidence of the measurement of PSD by averaging on a suitable number m of acquisitions, so the outcome of the averaging process is usually reported:

$$\langle S_x(f) \rangle_m = \frac{2}{T} \langle |X_T(f)|^2 \rangle_m \quad \text{for } 0 < f < f_s/2 \quad (1.4)$$

1.2 Basics of noise

In the development of a microwave frequency chain for the interrogation of narrow atomic transitions the noise becomes the first parameter of comparison and it is for this reason that a complete characterization of the noise processes will be performed. In this context it is useful to recall the most common noise processes affecting electronic oscillators.[2]

1.2.1 Phase and Frequency Noise

The quantities $S_\theta(f)$ and $L(f)$

The PSD of the random phase $\Theta(t)$, denoted with $S_\theta(f)$ and expressed in rad^2/Hz , is the quantity that characterizes the phase noise in the frequency domain.

Another way to express the phase noise is the $L(f)$, defined by IEEE Std 1139 – 2009 and expressed in dBc/Hz as

$$L(f)|_{dB} = 10 \cdot \log_{10}(S_{\theta}(f)) - 3dB \quad (1.5)$$

This is the formulation which will be used throughout this thesis, as all the used measurement devices adopt this standard. According to the above mathematical expression $L(f)$ and $S_{\theta}(f)$ are fully equivalent.[3][2]

The Polynomial Law

In most cases it is useful to describe the phase noise of oscillators and, in general, RF and microwave components by a polynomial model

$$S_{\theta}(f) = \sum_{n \leq -4}^0 b_n f^n \quad (1.6)$$

where the coefficients b_n are the parameters which quantify the corresponding noise process. Tab.1.1 reports the polynomial order for phase modulated (PM) and frequency modulated (FM) noise and Random Walk (RW), that are the most commonly encountered processes. Following the polynomial model, it is immediate to appreciate their impact on the measurement of phase noise and the regions in which their effect is predominant.

Noise Type	Phase noise $S_{\theta}(f)$	
	Law	unit
White PM	b_0	rad^2/Hz
Flicker PM	$\frac{b_{-1}}{f}$	rad^2
White FM	$\frac{b_{-2}}{f^2}$	$rad^2 \cdot Hz$
Flicker FM	$\frac{b_{-3}}{f^3}$	$rad^2 \cdot Hz^2$
Frequency RW	$\frac{b_{-4}}{f^4}$	$rad^2 \cdot Hz^3$

Table 1.1: Main processes of the polynomial law for phase modulated (PM) and frequency modulated (FM) noise and Random Walk (RW). Source: [Frequency and Amplitude Stability in Oscillators, CC BY E. Rubiola, 2019]

1.2.2 Thermal (Johnson) noise

Johnson-Nyquist noise is the electronic noise generated by the thermal agitation of charge carriers, typically electrons, within an electrical conductor in thermal equilibrium. This

is a noise that occurs independently of any applied voltage and becomes the fundamental limit in the sensitivity of a measuring instrument. Thermal noise increases with temperature. The power spectral density of this noise is given by Plank law

$$S(f) = \frac{hf}{e^{hf/kT} - 1} \quad (1.7)$$

where h is the Plank constant, T is the absolute temperature and k is the Boltzmann constant. At low frequencies, the Plank law is approximated with white noise of magnitude $S(f) = kT$. [2]

1.2.3 Shot noise

The shot noise is due to the fact that light or current can be described in terms of particles, photons and moving electrons respectively. The flux of these particles is not constant over time, but obeys a Poissonian statistics. Small fluctuations in their absolute number remain negligible as long as the number of particles is large, i.e. high light intensities, high currents. A ray of light has billions of photons, but if the number of photons per second is sufficiently decreased by varying the intensity of the beam, the relative fluctuations becomes significant and give rise to the shot noise.

Unlike thermal noise, shot noise is only present when electrical current flows, and it is independent of temperature and of the resistance of the electrical circuit. The PSD of the electric current noise is described by

$$S_I(f) = 2q\langle I \rangle \quad [A^2/Hz] \quad (1.8)$$

where q is the electron charge and $\langle I \rangle$ defines the average current. The standard picture for the electrical current is a stream of ϕ electrons per second emitted at random time, so the average current is defined as $I = \phi \cdot q$. [2]

1.2.4 Flicker noise

Flicker noise is also known as $1/f$ noise because its power density decreases with increasing frequency. The origin and physical mechanism underlying the Flicker noise is not clear and it is mostly described in an empirical way: usually in commercial devices the value of the corner frequency where flicker noise becomes dominant as compared to broadband white noise is indicated. The Flicker noise corner frequency f_c is the frequency where the magnitudes of the white and flicker noises of a device are equal.

1.2.5 Noise Figure

The noise figure is defined as the ratio of the output noise power of a device to the input noise power where the input noise power is attributable to thermal noise in the input termination at standard temperature T_0 (usually 290 K). For simplicity, the thermal noise is assumed to be white.

A less known definition was given by D.O. North (RCA Institutes, 1942), as the ratio of the output noise power from the transducer to the output noise power from an equivalent noise-free transducer. The problem with these two definitions is that they assume the same spectral distribution for the noise at the output and the input of the device, while in general the Signal to Noise Ratio (SNR) degradation may depend on the noise process to which the device is subject, and may not be the same at all frequencies. A more generic definition is hence given as *"The noise factor, at a specific input frequency, is defined as the ratio of the total noise power per unit bandwidth at a corresponding output frequency available at the output port when the noise temperature of the input termination is standard (290K) to that portion of engendered at the input frequency by the input termination."*[2]

1.2.6 Spurs

In frequency synthesis, the primary objective is always that of generating a signal that is a perfect sinusoid with no spurious. The presence of spurs in digital circuits depends on the quantization and their main frequency depends on the synthesized signal. In addition, RF components are often affected by spurs at the line cycle frequency (50 Hz) and its harmonics. Their presence can significantly affect the Cs spectroscopy readout in atomic clocks. Therefore, in our context, RF components and synthesis chains must be characterized with respect to these parameters as well.

1.2.7 Residual Noise analysis

In this paragraph, the measurement scheme used for the noise characterization is reported. To carry out a noise analysis of the chain it is necessary to measure the residual noise of each component. A residual phase noise setup isolates and measures a device's additive phase noise. This paragraph describes the procedure that has been followed for the characterization of the used components. This analysis is performed with a Phase Noise Analyzer.

The general scheme used to measure phase noise is shown in Figure 1.1. With Device Under Test (DUT) I indicate the element whose phase noise is to be measured. The basic idea is to duplicate the "chain": a signal generator generates a signal that is split into two arms with a power splitter; then, a copy of the element whose phase noise we want to measure is inserted in each arm (DUT1 and DUT2) in Figure.[4]

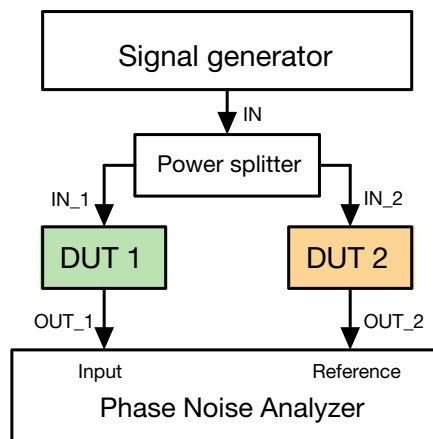


Figure 1.1: General scheme of a phase noise measurement. This measurement scheme will be used for almost all phase noise measurements

The Phase Noise Analyzer 5125A by Microsemi was used to measure the phase noise of the components. The measurement scheme is shown in Figure 1.2. It is based on digital sampling of the signal and on its subsequent processing. This digital approach guarantees higher dynamic range and flexibility than an analog-based set up.

The two input ports are indicated with "Input" and "Reference" and have a frequency range of 400 MHz. Both the signals entering on the DUT and the REF arm are filtered by an anti-aliasing filter to suppress harmonics, spurs, and broadband noise. The two filtered signals are split and sent to separate Analog to Digital Converters (ADCs). It is possible to distinguish two identical macroblocks, each performing the down-conversion and phase detection operation between the filtered and converted DUT signal and REF signal.[5]

The heart of the measurement is the down-conversion that immediately follows the ADC. The input signal is multiplied by the in-phase and quadrature component of a synthesized local oscillator and low-pass filtered. When the LO frequency is approximately equal to the input frequency, the output of the filters are in-phase (I) and quadrature (Q) base-band components of the input. The phase difference between the input signal and the synthesized LO is retrieved by computing the *arctangent* function of quadrature to in-phase components. Following the same process the down-conversion is performed on the REF channel. The subtraction process causes the phase noise of the instrument's clock oscillator to cancel, just as it does in a dual-mixer, phase difference, measurement system.

From each macroblock the phase of the signal (DUT or REF) is extracted and an algorithm calculates the cross-variance, while another algorithm calculates the spectrum and the cross-spectrum. In statistics and probability theory, the cross-variance or covariance

of two variables is a numerical value that provides a measure of their correlation.[6] The cross-spectrum indicates the correlation between the spectra of two signals in a frequency-domain perspective frequency.[7]

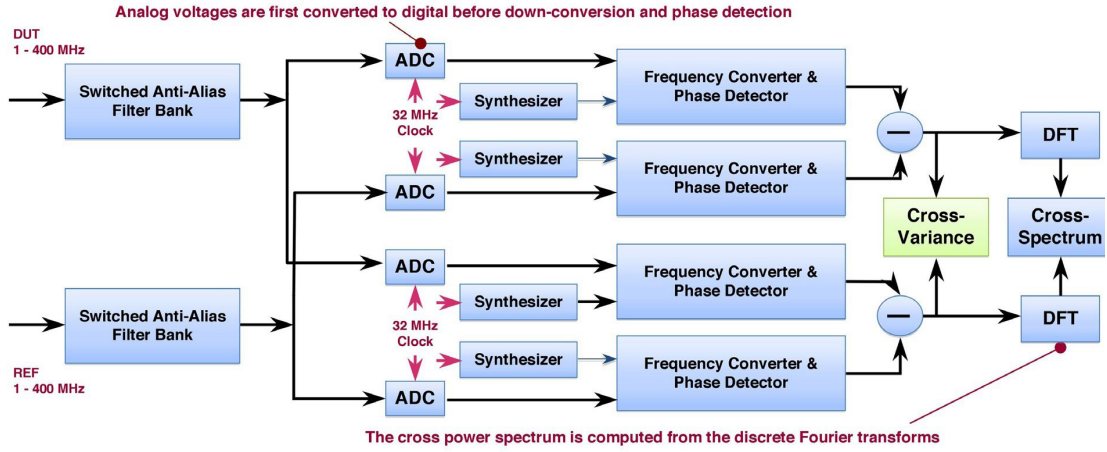


Figure 1.2: 5125A Microsemi Phase Noise Analyzer blocks scheme. Source: [5125 Datasheet]

1.3 Allan Deviation

In the characterization of oscillators and related components a time domain analysis of noise processes is usually performed, in addition to the more standard frequency-domain analysis. To this purpose, the most widely used estimator is the Allan Variance. It quantifies the instabilities of the DUT and allows an immediate understanding of both short-term and long-term behavior. Consider N data sampled with a sampling time equal to τ_0 . The entire data sampling interval can be divided into intervals (commonly called clusters) whose durations are multiple of the sampling time: $\tau_0, 2\tau_0, 3\tau_0, \dots, i\tau_0$. The Allan variance is obtained for each length of the clusters by the following formula:

$$\sigma_A^2 = \frac{1}{2K+1} \sum_{i=1}^{K-1} (\bar{\Omega}_{i+1} - \bar{\Omega}_i)^2 \quad (1.9)$$

where K is the number of clusters in the entire data sample, $\bar{\Omega}_i$ is the average of the values at the i^{th} -cluster. Unlike the classic variance, the Allan variance converges for all the common noise processes in oscillators. Furthermore, the dependence on τ varies according to the noise process that affects the measurement, so that a polynomial law similar to the one reported for the PSD can be found.[8]

Chapter 2

Caesium Fountain and Optical Comb

2.1 Caesium Fountain

2.1.1 Atomic Clock physical principle

Until 1967 the second was defined as the 86400th part of the mean solar day, that is the time interval between two successive passes of the Sun on the same meridian. This definition, which was considered imprecise, is now out of date. The second, since 1967, is defined as the time interval taken by a particular electromagnetic, emitted by Caesium atoms, to perform 9192631770 oscillations. As indicated by the International System, the second is defined as the *"time interval which contains 9192631770 periods of the radiation corresponding to the transition between the two hyperfine levels of the ground state of the 133 cesium atom"*. [9] The first atomic clock was realized by Louis Essen and Jack Parri in 1955.

To describe the basic operating principle of an atomic clock it is possible to describe the scheme in Figure 2.1. It is necessary to trace a local oscillator (LO) frequency to a reference, where the reference is provided by the frequency of a specific atomic transition, the clock transition. The probe radiation interacts with the atomic sample: if its frequency is reasonably close to the atomic reference atoms changes their atomic state. An active feedback control loop is implemented to maintain constant the frequency of the LO to the frequency resonance of the atoms. [10]

The best performing primary frequency standards are the Cs fountains, which are able to realize the second with a fractional frequency uncertainty in the low 10^{16} regime and show a white frequency noise instability in terms of Allan deviation of few parts in 10^{13}

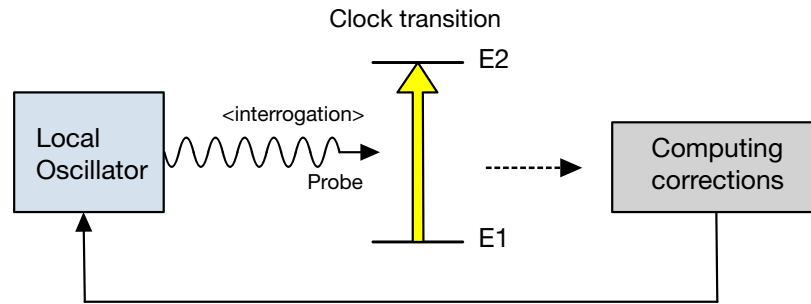


Figure 2.1: General scheme of an atomic clock. E1 is the fundamental state, E2 is the excited state

in 1 s averaging time.

The performance of the Cs clocks is now surpassed in terms of accuracy and stability by the other optical frequency standards (based on different atomic species as ytterbium, strontium, mercury, aluminum or magnesium).[10] In fact, a sample of ytterbium atoms was made at INRiM. Compared to atomic clocks, optical clocks reach lower statistical and systematic uncertainties and therefore could replace atomic clocks in the future for the redefinition of the second. In particular, the INRiM Yb standards has $3 \cdot 10^{-17}$ accuracy and stability $1 \cdot 10^{-15}$ at 1s.[12]

The atomic clock developed at INRiM in collaboration with the National Institute of Standards and Technology (NIST) is called IT-CsF2. The primary national standard at INRiM is characterized by an accuracy of $2 \cdot 10^{-16}$ and a stability of $2 \cdot 10^{-13} \tau^{1/2}$. Stability means statistical uncertainty (type A uncertainty) while accuracy means uncertainty of the systematic effects (type B uncertainty). IT-CsF2 fountain is shown in Figure 2.2.[11]

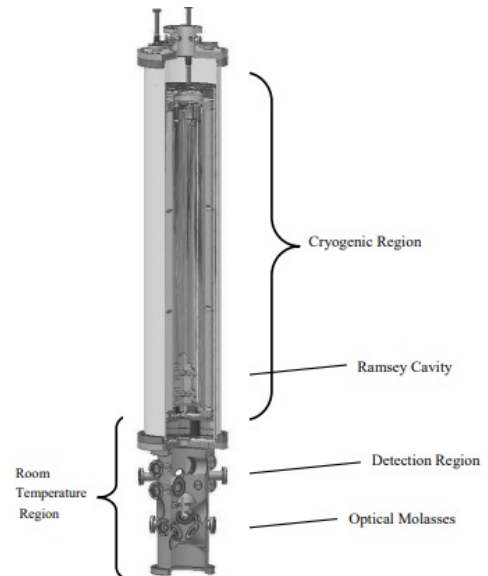


Figure 2.2: A cutaway drawing of IT-CsF2 showing the 1,1,1 molasses region, the detection region, and the cryogenic microwave interrogation region. The overall height is about 2.5 m. Source: ["NIST F1 AND F2" [11]]

The atomic sample is a cloud of cold Caesium atoms, slowed down and trapped in the

intersection area of six counterpropagating laser beams. The detection region, also at room temperature, is between the source region and the cryogenic, magnetically shielded Ramsey interrogation region and it is performed via fluorescence light of the atoms which have passed the Ramsey cavity twice.

Using an appropriate arrangement of laser beams and magnetic fields, it is possible to capture Caesium atoms, up to 1 million, from a thermal vapor and at the same time cool them down to a few micro-kelvins above the temperature of absolute zero. The newly cloud can be thrown against gravity using laser light. The name "fountain clock" is due to the similarity of this movement to that of water in a pulsed fountain. [13] Figure 2.3 shows the various operating stages during normal operation of the Cs fountain standard.

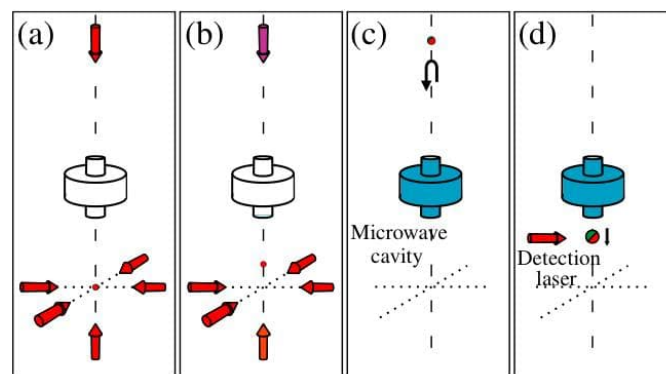


Figure 2.3: Fountain clock description. Source: [Atomic fountain clocks - R. Wynands, S. Weyers - <https://iopscience.iop.org/article/10.1088/0026-1394/42/3/S08>]

- (a) The cloud of atoms is trapped in the intersection area of six laser beams;
- (b) the cloud is launched by frequency detuning of the vertical lasers;
- (c) the cloud slowly expands during its ballistic flight. It passes through a microwave cavity, here the first interaction with happens. A second interaction happens when the atoms fall down under the effect of gravity;
- (d) detection lasers are switched on, they probe the population distribution by laser-induced fluorescence. From this measurement, the detuning of LO with respect to the atomic resonance is calculated and its frequency is corrected to keep it on resonance.

The interrogation follows a Ramsey scheme: atoms interact with a microwave (local oscillator, LO) tuned at the nominal resonance frequency a first time on the way up, and a second time on the way down. During the interactions, the atoms wave function evolves freely. If the LO is on resonance, it is expected that after the second interaction all atoms are in the excited level, while the transition probability decreases as the detuning of LO

from resonance increases. After the second interaction, a laser (detection laser in the Figure 2.3) illuminates the atoms and allows measuring how many atoms performed the transition. From this measure, it is possible to calculate the detuning and correct the LO frequency to bring it on resonance. This quantity is used as frequency discriminator to realize the clock. The procedure is continuously repeated. The atomic response in frequency is an interference fringe pattern, where the fringe width, of order of 1 Hz, is inversely proportional to the time spent above the Ramsey resonator.[14] The 2-stage Ramsey interrogation allows a much higher resolution as compared to a traditional Rabi interrogation. The probability of particles' transfer describes the well-known Ramsey fringes.[15]

2.1.2 Dick effect and Noise budget

A serious limitation of the short-term stability of an atomic fountain clock is given by the phase noise of the local oscillator at 9.192631770 GHz interrogating the atom sample. Any phase excursions of this oscillator, while no atoms are in or above the microwave cavity, will go not be seen by the atoms, meaning that it will not be corrected in the feedback loop and therefore will result in additional phase noise at clock output. This is what is called Dick effect. In order to reduce its influence, it is possible reduce the dead time of the fountain speeding up the loading and preparation of the cold atomic cloud but unfortunately, some dead time is unavoidable in a standard pulsed fountain because one has to wait until the detection process is finished before the next cloud can be launched. The easiest way to reduce the influence of the Dick effect on the short-term instability is using local oscillator with the lowest phase noise.

At high density the short term stability of IT-CsF2 is typically $2 \cdot 10^{-13} \tau^{-1/2}$, while at low density the stability is typically reduced by a factor 2. This data will be taken up later to compare it with the value of the new chain.

2.1.3 Microwave synthesis chain

The goal is to design a low noise synthesis chain with a stable low noise LO to reduce the Dick effect. A simplified schematic of the chain is reported in Figure 2.4. The important elements are the hydrogen maser, the high-quality (BVA) quartz oscillator, the synthesizer and the time-difference measurement unit. The Maser is the reference oscillator for the chain, used as secondary standard which is calibrated/characterized by the Cs fountain. Moreover the maser, thanks to his continuous operation, is the official source of the italian reference time.

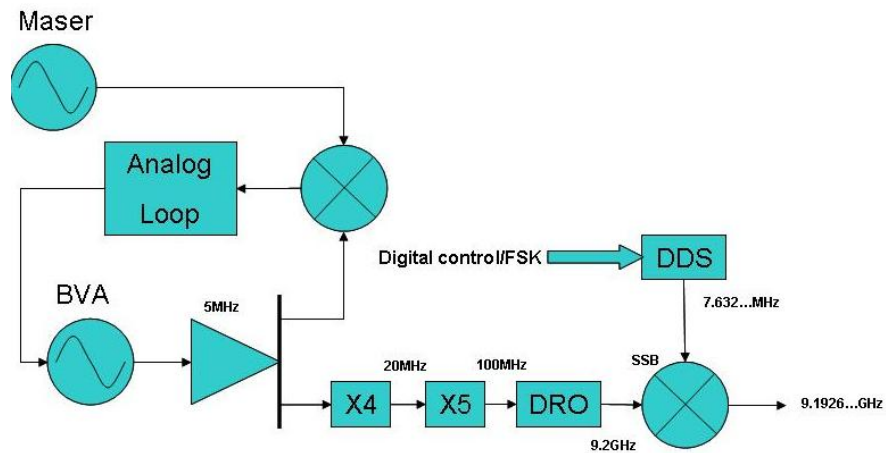


Figure 2.4: Scheme of the synthesis chain used in ITCsF2. Source:[Accuracy evaluation of ITCsF2: a Nitrogen cooled Caesium Fountain - Levi, Calonico, Calosso, Godone, Micalizio, Costanzo]

It generates a reference signal at 5 MHz. At short times the fountain stability is supported by the excellent stability of the BVA quartz, while at longer times the quartz is locked to the maser, which has better stability in the long term. The 5 MHz produced by the BVA quartz is multiplied by 4 and then multiplied again by 5; the generated 100 MHz sent to a Dielectric Resonator Oscillator (DRO) that generates a signal at the frequency of 9.2 GHz. This signal is mixed with the signal of a DDS at ≈ 7.37 MHz to produce the 9.192631770 GHz microwave signal which is sent to the microwave cavity. Two identical synthesizers were developed, one for the Ramsey excitation and one to feed the state selection cavity.

Undesired shifts from spurious components are excluded, since the only detected components are at 50 Hz and its harmonics, whose power is highly symmetric with respect to the carrier.[12]

2.2 Optical Frequency Comb

Currently, low-noise microwave sources are based either on ultra-low noise quartz oscillators or on cryogenic sapphire oscillators. The latter is not commercially available and has high maintenance costs; on the other hand, even the best quartz oscillator sources may not have sufficiently good performances for cutting-edge applications. By combining an ultra-stable laser with the Optical Frequency Comb (OFC) it is possible to synthesize signals with phase noise performance that surpasses all existing microwave sources over a wide range of the Fourier spectrum. An optical comb is a mode-locked laser, i.e. a pulsed laser source characterized by discrete emission modes that have a fixed phase-relation. This results in ultra-short pulses with femtosecond duration.[16] Thanks to this property the OFC allows the direct conversion of frequencies from the optical to the microwave domain and vice-versa, allowing the extraction of microwave signals referenced to optical atomic clocks. When a specific mode of the OFC is phase locked to an ultra-stable continuous-wave laser, the synthesis of microwave signals is possible through the photodetection of light pulses with a fast photodiode and this enables high-fidelity frequency transfer to the mid-infrared, terahertz, and microwave domains. In the following paragraphs, it will be shown that the produced microwave will copy the spectral purity of the optical reference signal.

The repetition time of light pulses in the comb is usually 4 ns. In a frequency-domain perspective, this corresponds to a series of RF modes 250 MHz apart from each other. In particular, the frequency of each comb mode can be described as

$$\nu_N = N \cdot f_r + f_o \quad (2.1)$$

where N is an integer of order of 1 million, f_r is the repetition rate and f_o is a constant offset frequency that depends on the comb internal structure.

It is expected that when the optical comb is combined with a single-frequency laser a pair of beat notes whose frequency is less than 250 MHz will always be detected on a photodiode, i.e. the beat notes of the laser with the two adjacent optical modes. Since the modulating frequency is < 125 MHz (i.e. half of the comb repetition rate), it will be visible on a Spectrum Analyzer and can be measured with high precision with electronic devices. If the absolute frequency of the comb tooth is known, it is possible to determine also the absolute frequency of the laser. In particular, measuring the beat note of a laser with the closest comb mode and denoting it as f_{beat} , the laser frequency can be written as

$$\nu_{laser} = N \cdot f_r + f_o + f_{beat} \quad (2.2)$$

In this equation, there are only two degrees of freedom: the repetition rate f_r and the

offset frequency f_o .

This ability to uniquely define the frequency of a laser in terms of microwave frequencies allows the absolute frequency of any laser to be determined with up to 10^{-18} accuracy by single beat note measurement. In addition, instead of using it as a "ruler" to perform absolute frequency measurements, the comb can be used to synthesize low-noise microwave. In this case, the comb mode closest to the laser is phase-locked to it by adjusting the repetition frequency. By inverting equation 2.2 it is possible to see that the frequency fluctuations of the repetition rate will be equivalent to those of the laser, scaled by the factor N . Because N is of the order of the ratio ν_{laser}/f_r , then $\frac{\Delta f_r}{f_r} \approx \frac{\Delta \nu_{laser}}{\nu_{laser}}$, i.e. if an ultra-stable laser with instability 10^{-15} is used as a reference, it will be possible to extract a microwave with the same relative stability, surpassing that of standard microwave oscillators.[16].

The microwave synthesis unit is obtained in an external module provided by the comb manufacturer, Menlo System. A picture of the module and the corresponding block diagram are shown in Figure 2.6 and in Figure 2.5.

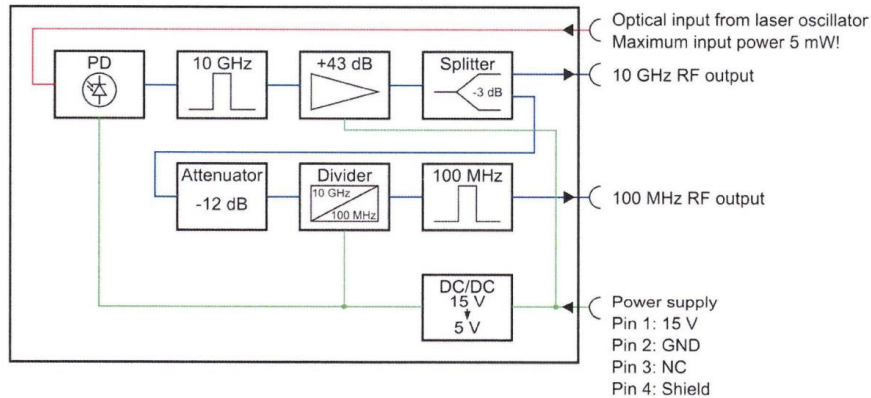


Figure 2.5: Menlo System 10GHz/100MHz RF generator schematic. The schematic shows the path of the signal deriving from the Optical Frequency Comb in red, it is an optical fiber connection; the electrical RF connections are shown in blue; in green the power supply connections.

The pulsed comb output is sent to an internal fast photodiode with a bandwidth larger than 10 GHz. Because the pulses have a repetition time of 4 ns, the photodiode output will give rise to many spectral lines at a distance of 250 MHz from each other. The low-level output signal of the microwave extraction photodiode is filtered by an ultra-low insertion loss microwave filter and amplified. The amplified signal is split by a Power Divider: one output is sent to the 10 GHz output of the module (B in Figure 2.6), the

other output is attenuated by 12 dB and divided by a factor of 100 thus generating an additional output at a frequency of 100 MHz (A in Figure 2.6) which is not used in this context.[17] Thanks to the photodiode it is possible to extract the 40th harmonic of the repetition rate at 10 GHz. This microwave, sent to the chain, will be converted to 9.192 GHz.

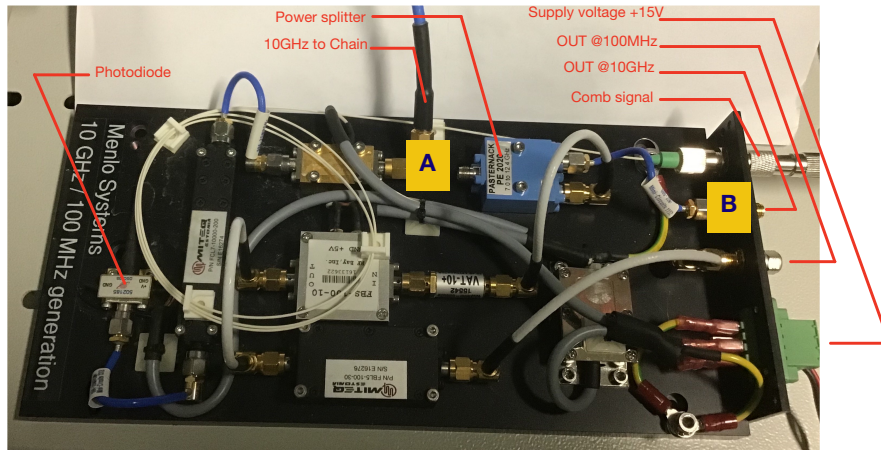


Figure 2.6: Menlo System 10GHz/100MHz RF generator photo

Chapter 3

Chains Design: 10 GHz to 9.192 GHz

The goal is to create a low-noise synthesis chain capable of generating a microwave at a frequency of 9.192 GHz starting from the 10 GHz input signal derived from the optical comb. The generated microwave will be used to interrogate the Cs atoms in the fountain. In the design of the chain, it is necessary to keep in mind that its contributed noise has to be negligible compared to the intrinsic noise of the microwave itself. The new chain should feature a better spectral purity, between 1 Hz and 10 Hz, than the synthesis chain currently used.

Using dividers, multipliers and Direct Digital Synthesizer (DDS), various design possibilities exist but the design has to integrate the lowest number of elements, and each of them must exhibit a suitably low noise level. Here, I will focus in particular on two specific designs that use the minimum number of components. The main difference between the two lies in the use of both analog and digital components (DDS board) in the first and only analog components in the second.

The DDS enables to synthesize arbitrary waveforms from a single, fixed-frequency reference clock. DDS components are present in applications such as signal generation, local oscillators in communication systems, function generators, mixers, modulators, sound synthesizers, and as part of digital phase-locked loops. A DDS has many advantages over its analog counterpart, the analog prescalers and multipliers, including much better frequency agility, improved phase noise, and precise control of the output phase across frequency switching transitions. Disadvantages include spurious responses mainly due to truncation effects, crossing spurs resulting from high order (>1) Nyquist images, and a higher noise floor at large frequency offsets mainly due to the digital-to-analog converter.[18]

The advantages and disadvantages of each of the two chains will be taken into consideration to choose the best one. On the basis of a lower noise contribution, the number of components can increase the overall temperature sensitivity of the chain and possibly introduce additional phase noise.

In the remainder of this chapter, I will first report on the characterization of the Phase Noise Analyzer that I used for the measurements, and then of each single component within the chain. On the basis of the residual noise contributed by each component, the noise budget of the complete chain will be computed, and compared with the measured noise obtained by comparing two entirely identical chains. In addition to reporting the phase noise curves of each chain, it is interesting to pay attention to another detail: the harmonics. It is important to consider all the harmonics that are not filtered by the fountain cavity. A critical requirement for the fountain operation is that their power in the bandwidth of the microwave cavity, i.e. 200 kHz, must be at least 60 dB lower than the 9.192 GHz carrier, not to affect the clock operation. This condition guarantees the absence of any microwave-induced shift on the atomic levels and hence avoids systematic errors on the Cs transition frequency measurement with the fountain clock. The two chains will also be compared in terms of stability using the Allan deviation curves.

3.1 Characterization of Phase Noise Analyzer

The used Phase Noise Analyzer is the *Microsemi 5125A* whose principle of operation was described in section 1.2.7. To characterize the measurement noise floor of the phase noise analyzer I adopted the general scheme reported in Figure 1.1: a signal with a power of 13 dBm and frequency 100 MHz is generated, split by means of a power splitter, and the two outputs are sent to the "Input" and "Reference" channels of the Phase Noise Analyzer.

The measurement results are shown in Figure 3.1: it is possible to identify a white noise with a PSD of -168 dBc/Hz, while a flicker phase noise emerges for frequencies below 1 kHz.

The measured phase noise level will represent the noise floor for subsequent measurements. As will become evident later, this level is suitable for our purpose, as it is low enough not to limit the noise measurement of the chains.

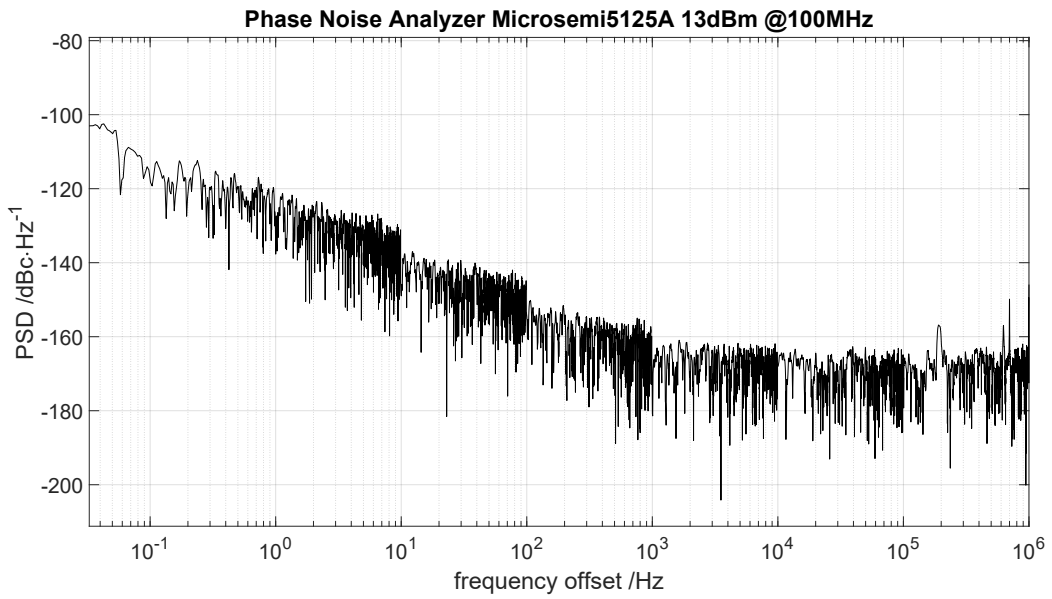


Figure 3.1: Phase noise of Phase Noise Test with an input signal of 13 dBm split into two signals. These two signals are sent as input and reference for the phasometer.

3.2 First Chain

The block diagram of the complete chain is shown in Figure 3.2.

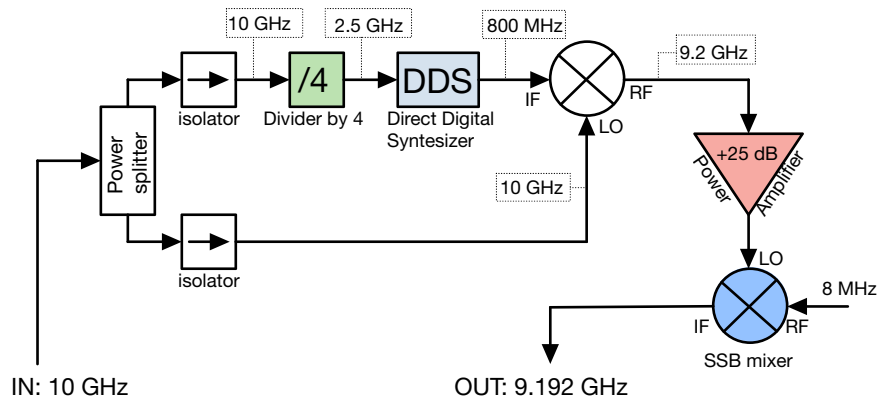


Figure 3.2: Complete first chain: from 10 GHz to 9.192 GHz

The chain takes as an input signal the 10 GHz signal generated by the optical comb. This is split into two arms, one of which is scaled down to 800 MHz. The produced signal

will then be used to down-convert the 10 GHz signal to 9.2 GHz using a high-bandwidth frequency mixer. The arm that is used to generate the 800 MHz signal contains a divider by 4 and a DDS board. The divider by 4 is used because the DDS admits an input signal with a maximum frequency of 3.5 GHz. It was, therefore, appropriate to divide the input signal by 4 to obtain a signal at 2.5 GHz. The 9.2 GHz signal is mixed with a 8 MHz signal generated externally by a Single Sideband Mixer. The component is the IROH-04-458. It is a 4-ports device, with 2 inputs, and 2 output. When a RF signal is applied to either the IF1 or IF2 ports, the mixer generates the upper or lower sideband of the LO respectively, while rejecting the other. The SSB is used to generate a 9.192 GHz signal rejecting the 9.208 GHz sideband. It requires a power level of approximately 10 dBm on the LO input, therefore the 9.2 GHz signal is amplified by the WNA-220 amplifier by a 25 dB factor.

3.2.1 Characterization of Divider by 4

The frequency divider by 4 is the Hittite HMC365G8. It has a specified phase noise equal to -151 dBc/Hz, input bandwidth ranging between 0.2 GHz and 14 GHz. 7 dBm output power and 5 V DC power supply. The phase noise of the divider is measured by adopting the general scheme shown in Figure 1.1, with two, nominally-identical copies of the same divider model representing DUT1 and DUT2. Since the Phase Noise Analyzer admits an input signal with a maximum frequency of 400 MHz the input signal frequency is set to 1.6 GHz. The two 400 MHz output signals are sent to "input" and "reference" channels of the Phase Noise Analyzer.

To evaluate the frequency dependence of this component a second measurement is done with a 800 MHz input signal to generate an output signal of 200 MHz. The two measurements are shown in Figure 3.3 (black and blue curve respectively).

It is possible to notice that the two curves overlap even though the input frequency is different. It is then possible to conclude that the phase noise of the divider does not depend on the input frequency, and for this reason, it will be the same also in the operative condition, where a 10 GHz input signal is divided to generate a 2.5 GHz signal.

Assuming that the noise of DUT1 and DUT2 is identical in power but uncorrelated, the noise of each divider is expected to be 3 dB lower than the level shown in Figure 3.3. The measured white noise level is consistent with the one specified in the datasheet (-151 dBc/Hz) for a single component, while no specification was available in the datasheet concerning the flicker noise component.

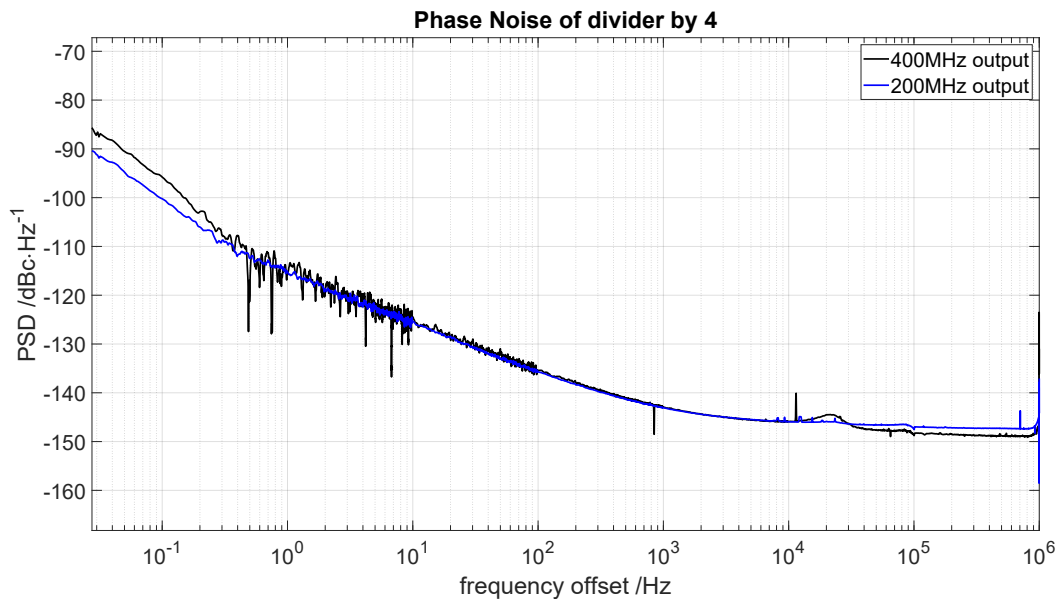


Figure 3.3: Phase Noise of Divider by 4. In blue: input signal at 800 MHz and an output signal at 200 MHz; in black: input signal at 1.6 GHz and an output signal at 400 MHz

3.2.2 Characterization of the DDS

The DDS component is the Analog Devices AD9914. It features 3.5 GSPS internal clock speed, integrated 12-bit DAC, frequency tuning resolution to 190 pHz, 16-bit phase tuning resolution, 12-bit amplitude scaling, programmable modulus, phase noise equal to -128 dBc/Hz at 1 kHz offset with 1396 MHz input frequency and 1.8 V/3.3 V power supplies. In the chain the DDS must generate a signal at 800 MHz, but with the measurement scheme of Figure 1.1 it is not possible to measure the phase noise at this frequency due to the limited bandwidth of the Phase Noise Analyzer. For this reason, two measurements are performed by synthesizing 200 MHz and 400 MHz. As in section 3.2.1 this process allows us to evaluate the frequency dependence of the noise and infer the noise that will be obtained in the final operating conditions. The phase noise of the two measurements is shown in the Figure 3.4.

In the region of the Fourier spectrum dominated by flicker noise an increase of 6 dB is measured as the output frequency doubles. The frequency dependence of the white noise is instead less pronounced: the white level at 300 kHz is -144 dBc/Hz for the measurement of 200 MHz output signal, and -147 dBc/Hz for the measurement with 400 MHz output signal.

For an in-depth interpretation of the obtained results, and in order to confirm the frequency dependence we compare our results to those reported in the datasheet. Here, the DDS

residual noise is shown for an output frequency of 1396 MHz. From the black curve in the figure, at 1 kHz the noise is -133 dBc/Hz. Assuming, as before, that the noise of the two identical copies of the DDS are identical and uncorrelated, and hence that the noise of each component is 3 dB lower than those reported in Figure 3.4, 3 dB are subtracted from -133 dBc/Hz. Assuming that the measured flicker noise scales proportional to the output frequency, a residual contribution at 1 kHz of -136 dBc/Hz + $[20 \cdot \log_{10}(1396/400)]$ dB = -126 dBc/Hz would be expected for a 1396 MHz synthesized output signal. This value is comparable with the value reported on the datasheet (-128 dBc/Hz at 1 kHz).

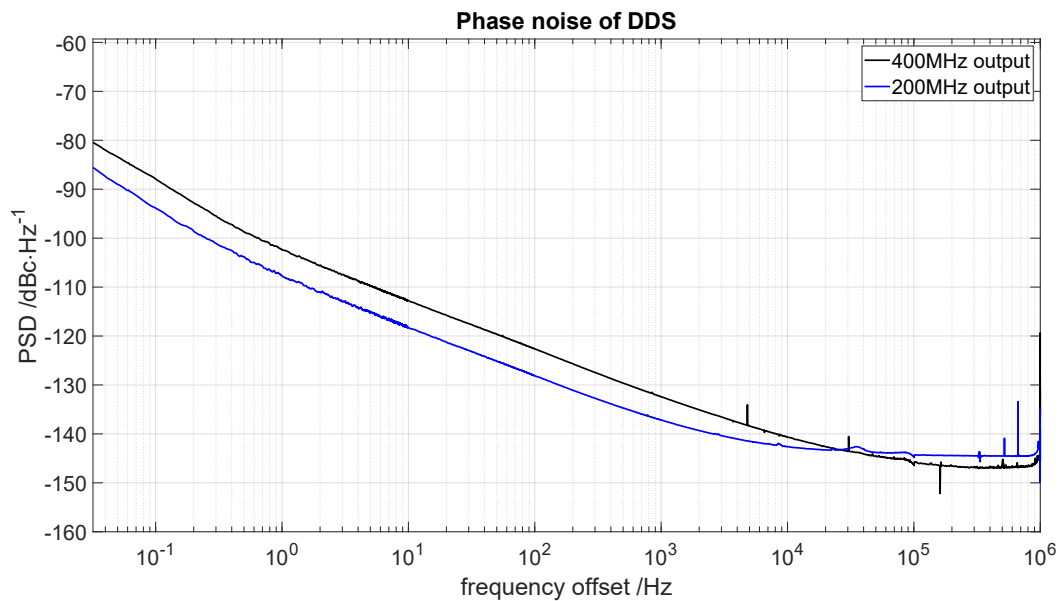


Figure 3.4: Phase Noise of DDS. In blue: the input signal is at 2.5 GHz, the output at 200MHz; in black: the input signal is at 2.5 GHz, the output at 400 MHz

3.2.3 Characterization of Amplifiers

Two kind of amplifiers are used: the WNA-220 by RF-bay and the ZKL-1R5+ by Mini-Circuit. The former is an High frequency Amplifier with 10 MHz-10 GHz bandwidth and a gain factor of 25 dB, the latter a low-frequency amplifier with 10 MHz-1500 GHz bandwidth and a gain factor of 41 dB. The two amplifiers are used in two different parts of the chain. Thanks to its higher bandwidth, the WNA-220 is used to amplify the mixer output signal at 9.2 GHz and to amplify the RF output signal of the image-rejection mixer; even if the ZKL-1R5 amplifier is not strictly used in the synthesis chain, it is used for its characterization as will be described in the next paragraph. It is then convenient to report here on its characterization, by comparison with the WNA-220, also because the measurement scheme is the same. The configuration shown in the Figure 3.5 is used to

characterize the two amplifiers.

The WNA-220 amplifier is characterized using an input signal with frequency equal to 200 MHz in a first measurement and 400 MHz in a second one with a power equal to 8 dBm. This is split into two branches: one output of the power splitter reaches the amplifier, a second output directly reaches the "reference" channel of the Phase Noise Analyzer. Since the input signal of the amplifiers is 2 dBm a 20 dB attenuator is added to avoid saturation.

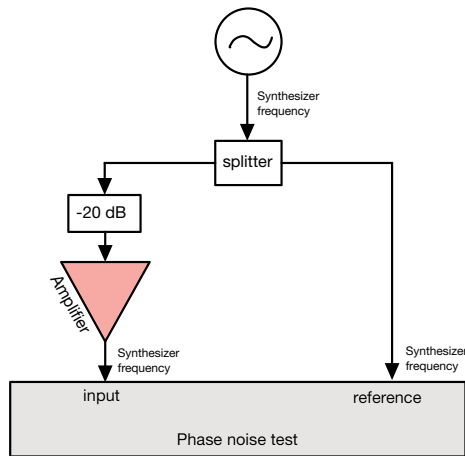


Figure 3.5: Block Chain for amplifiers phase noise measurements

The ZKL-1R5 amplifier is characterized using the same model: the two measurements are done with a 100 MHz and a 200 MHz signals. As the amplification factor is 41 dB a 40 dB attenuator is used at the input to avoid output signal reaches saturation instead of a 20 dB attenuator as shown in the figure.

Figure 3.6 shows the phase noises relative to the ZKL-1R5+ amplifier with a 100 MHz and 400 MHz signal, while Figure 3.7 shows the phase noises relative to the WNA-220 amplifier with a 200 MHz and 400 MHz signal. In both cases, in the flicker region, the measured noise level is limited by the noise floor of the PNA. Thus, we can assume they represent an upper limit to the noise of the two amplifiers. The noise of the two amplifiers does not depend on the frequency of the input signal.

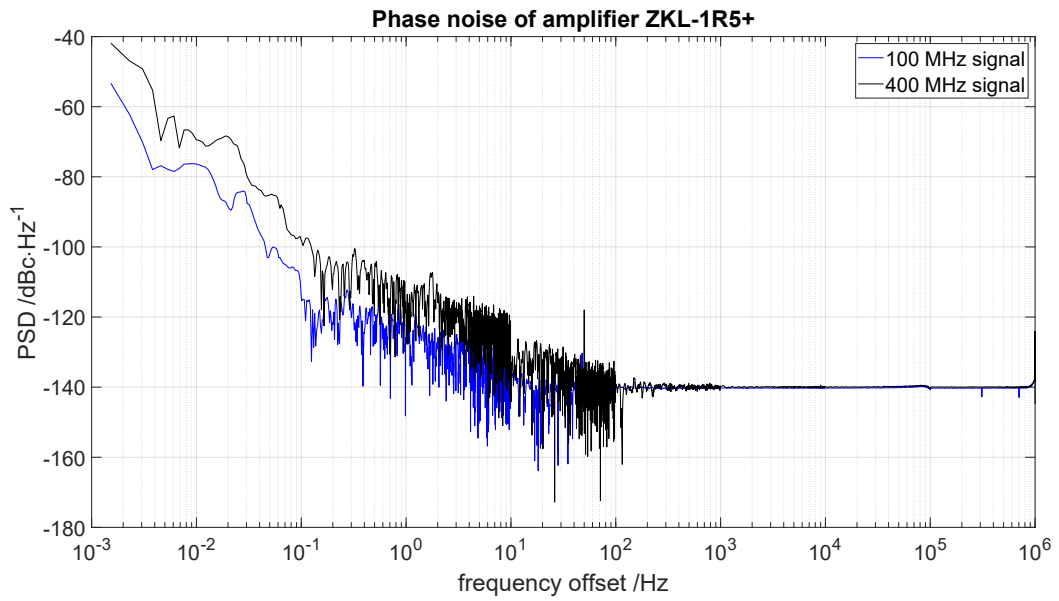


Figure 3.6: Phase Noise of Amplifier ZKL-1R5+: in blue at 100 MHz, in black at 400 MHz

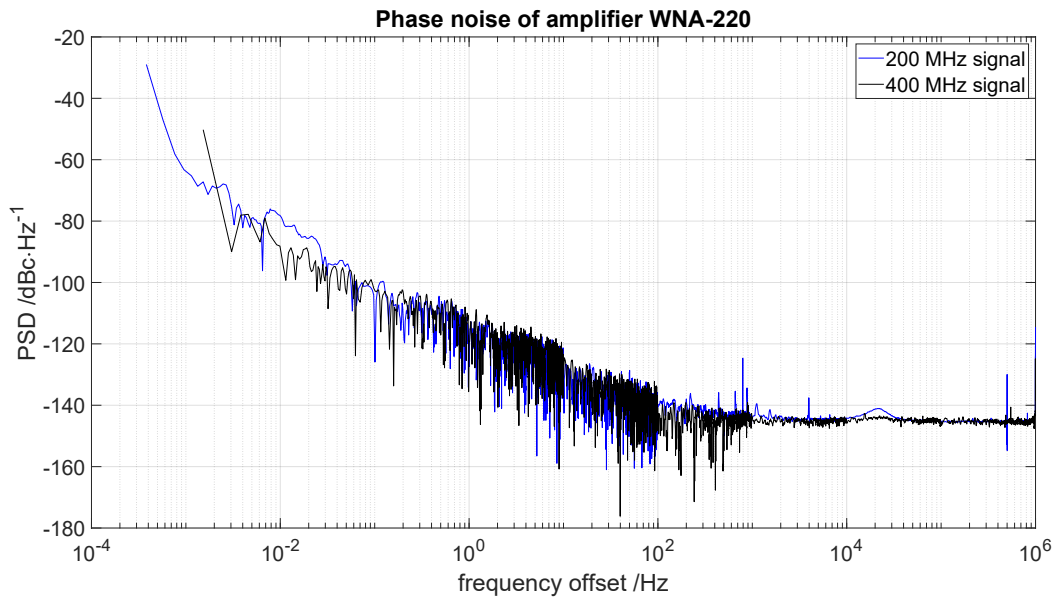


Figure 3.7: Phase Noise of Amplifier WNA-220: in blue at 200 MHz, in black at 400 MHz

3.2.4 Characterization of Single-Sideband Mixer

As other mixers, the image-rejection mixer suffers mainly from thermal noise. In our configuration, given the relatively high driving power, this process is negligible. On the other hand, an important figure of merit is the cross-talk between the input and output port: for this characterization it is sufficient to use a spectrum analyzer.

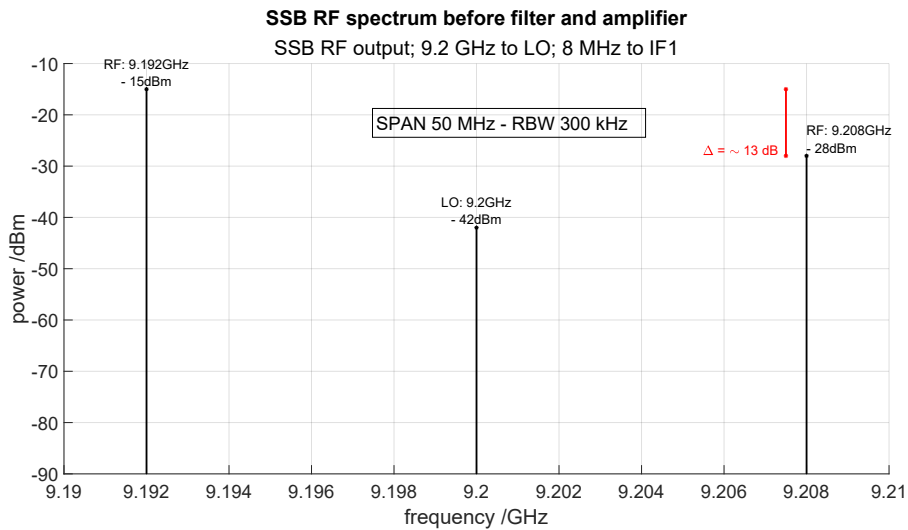


Figure 3.8: 8 MHz to IF1 channel

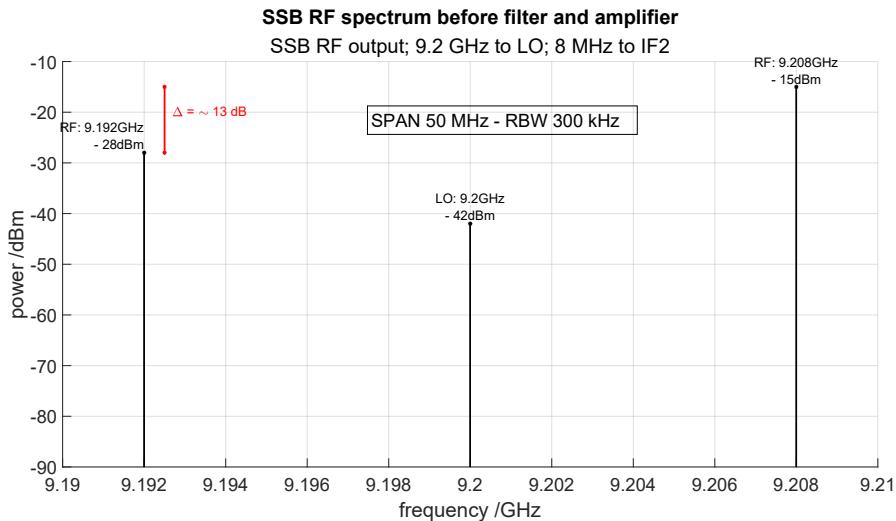


Figure 3.9: 8 MHz to IF2 channel

Figure 3.8 and Figure 3.9 show the RF spectrum obtained at the mixer output by applying a 8 MHz signal to the IF1 and IF2 ports, when the LO frequency is 9.2 GHz. The presence of leakage from the LO is also observed at 9.2 GHz. The undesired sideband is attenuated by 13 dB.

3.2.5 Noise of the complete chain

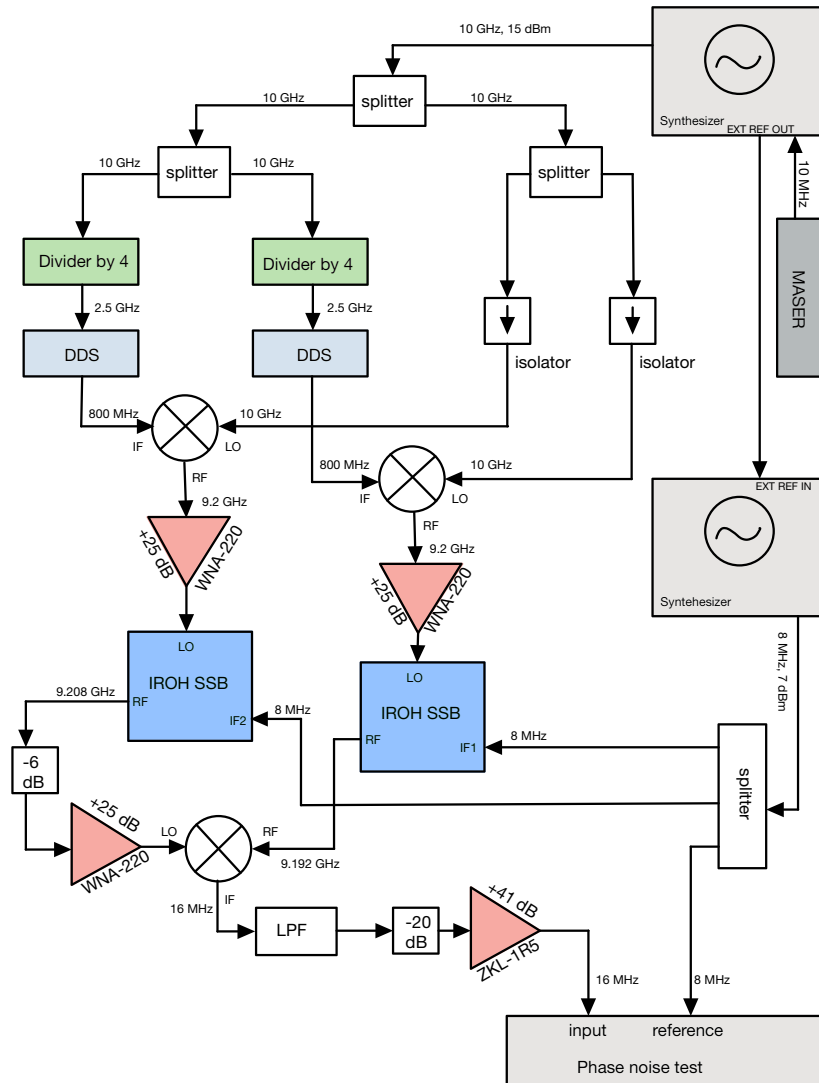


Figure 3.10: Complete first chain: from 10 GHz to 9.192 GHz

After characterizing individual components, we build two identical copies of the chain following the scheme on Figure 3.10, to measure its overall contributed noise. To perform the measurement the chain was duplicated, while keeping the same 10 GHz oscillator as a seeding signal. For this reason, an additional splitter is used, and the power of the 10 GHz input signal is increased to compensate the additional loss.

Starting from a signal at the frequency of 9.2 GHz in each chain it is possible to obtain a signal at the frequency of 9.192 GHz or 9.208 GHz by mixing it with a 8 MHz LO and selecting the lower or higher sideband. The 8 MHz signal is then split into three signals: two of them are sent to two Single-Sideband (SSB) mixers that generate the two sidebands, the third one is sent to "reference" channel of the Phase Noise Analyzer. The noise contribution of the image rejection mixer is negligible. The two are mixed together, and the difference signal at 16 MHz is filtered, attenuated by 20 dB, amplified with a *ZKL – 1R5* amplifier and sent to the "input" channel of the Phase Noise Analyzer. In this way, it is possible to reject both the noise of the master LO at 10 GHz and of the LO at 8 MHz, and measure the combination of the residual noise of the two chains.

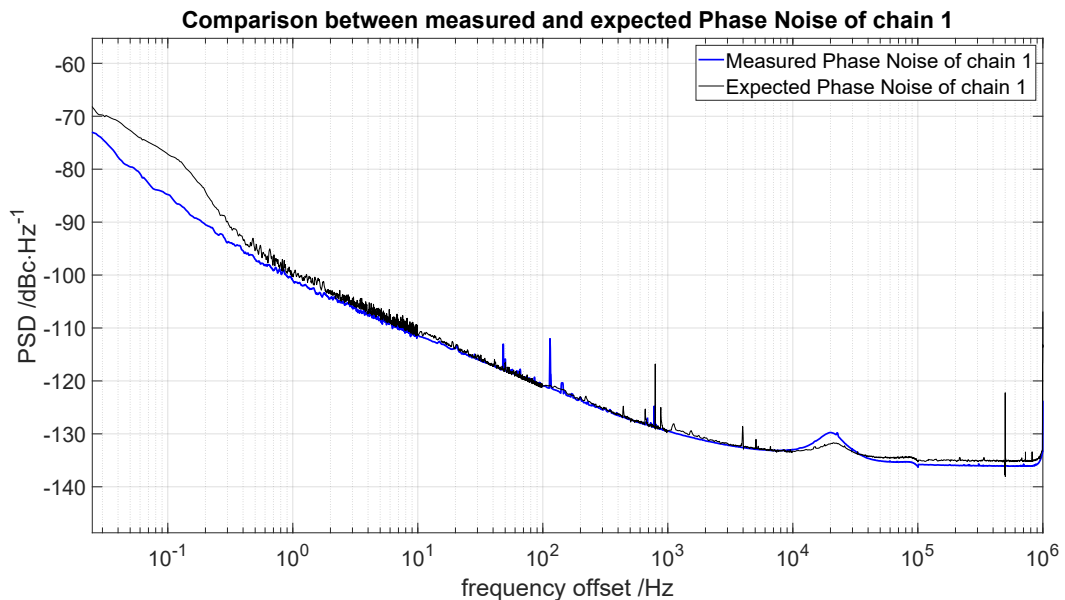


Figure 3.11: Residual noise of the first chain, generating a 9.192 GHz microwave from a 10 GHz signal. 3 dB have been removed from the raw measurement to take into account that two identical chains were compared

The measurement result is shown in Figure 3.11 (blue curve), and is compared to the expected noise for this chain (black curve), obtained by combining the residual noises of the individual components within the chain suitably scaled according to their dependence on the frequency of the input signal. In the calculations, 3 dB were subtracted

from the values reported in the previous section for individual components in the case the measurement followed the scheme shown in Figure 1.1, as the measurement was performed doubling the chain and assuming that the two identical chain contributes equally to the noise. The measured noise in Figure 3.11 represents the combined noise of the two chains, while the noise of the single chain is expected to be 3 dB lower. From the figure it is therefore possible to observe that the white noise is about -135 dBc/Hz limited by limited by the residual phase noise of the WNA-220 amplifier, while at 1 Hz, flicker noise is about -100 dBc/Hz at 1 Hz limited by the residual phase noise of the DDS.

As mentioned earlier, an importance aspect to characterize is the presence of spurious signal in bandwidth of 200 kHz that is the bandwidth of the microwave cavity. A fundamental requirement to interrogate the Cs atoms in the fountain correctly is that the power of spurious is at least 60 dB lower than the carrier. As a first step, we asses the presence of spurious signals around the carrier at 9.192 GHz with a span reduced to 500 Hz and a resolution bandwidth (RBW) equal to 1 Hz. The Figure 3.13 shows the fundamental frequency 9.192 GHz with the spurs generated by the entire chain. From the Figure, it is possible to see that the closest spur at 50 Hz is about 62 dB lower the carrier.

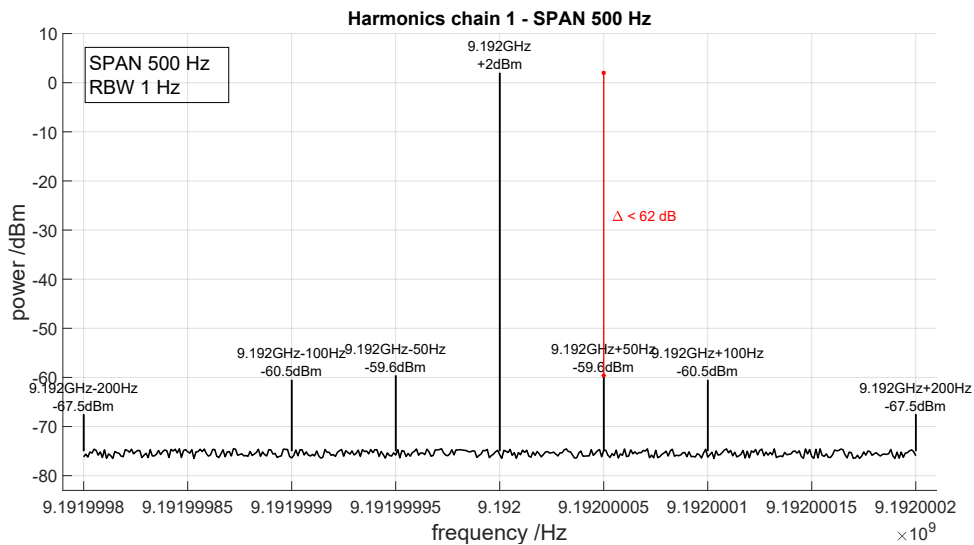


Figure 3.12: Harmonics of chain 1 with a SPAN of 500 Hz

Then, the span is extended up to 200 kHz with a RBW of 300 Hz and spurious are observed on a wider bandwidth. Spurious signals are observed at 779 Hz, 10.35 and 15.15 kHz from carrier. The highest one, at 779 Hz, is 68 dB lower than the carrier, We can thus conclude that both for large and small span, the chain fulfils the requirement.

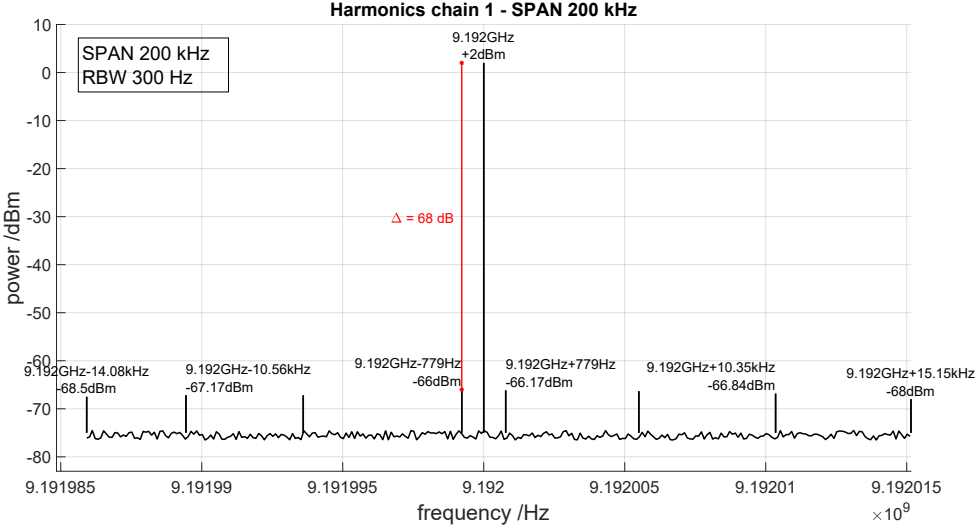


Figure 3.13: Spurs of chain 1 with a SPAN of 200 kHz

3.3 Second Chain

In the second chain the divider by 4 and the DDS are replaced by a divider by 25 and a multiplier by 2. The block diagram of the complete chain is shown in Figure 3.14. The 10 GHz input signal is divided by 25 generating a 400 MHz signal and then multiplied by 2 to generate an 800 MHz signal which is mixed with the same 10 GHz signal to generate a 9.2 GHz signal. The 9.2 GHz signal is sent to the LO input channel of the SSB and is mixed with an 8 MHz to generate a 9.192 GHz.

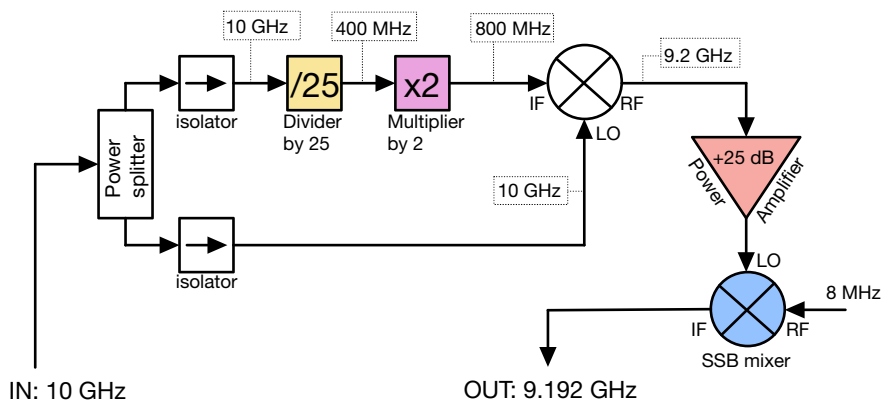


Figure 3.14: Complete second chain: from 10 GHz to 9.192 GHz

In the discussion of the second chain we focus only on the differences between the first chain and the second, i.e. the divider by 25 and the multiplier by 2.

3.3.1 Characterization of Divider by 25

The divider is the FBS-25-14 by RF Bay. The measurement scheme follows the reference scheme reported in Figure 1.1. An input signal with power of 8 dBm and frequency of 10 GHz is split into two branches, each one routed to a frequency divider, and the output signals at 400 MHz are sent to the two channels of the Phase Noise Analyzer.

The phase noise of the measurement is shown in the Figure 3.15. At 1 Hz the phase noise is -105 dBc/Hz. The measured level of white noise is consistent with the specified noise of -145 dBc/Hz found on the datasheet, considering that 3 dB must be removed from the shown results to account for the presence of two dividers in the measurement setup.

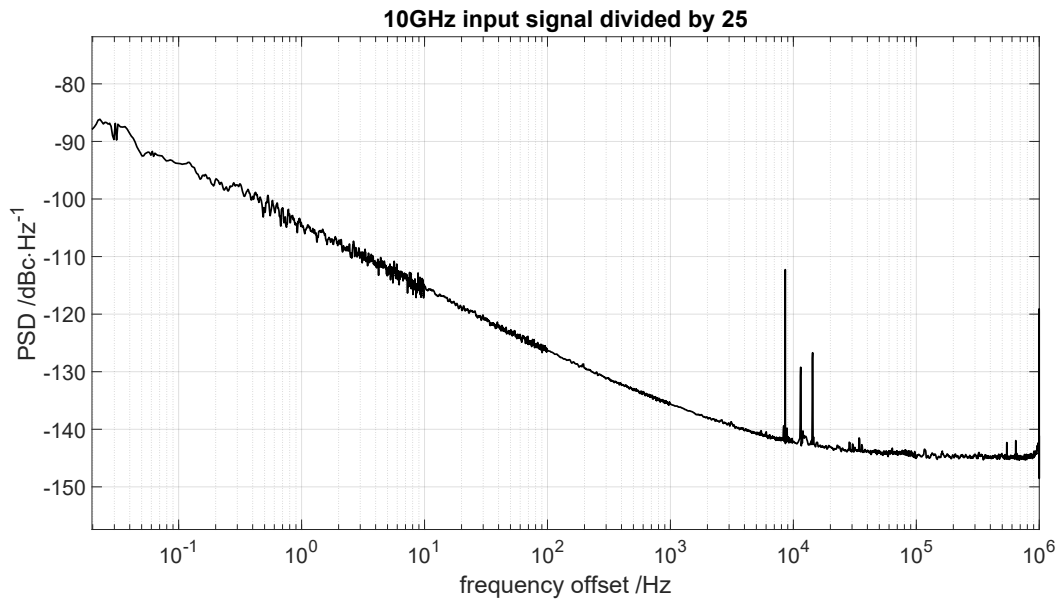


Figure 3.15: Phase noise of divider by 25 RF-BAY FBS-25-14 at 10 GHz

3.3.2 Characterization of Multiplier by 2

The second component of the chain is the multiplier by 2, ZX90 – 2 – 13 – S + by Mini Circuit. This is driven by the 400 MHz output of the divider; the multiplier generates a signal at the frequency of 800 MHz. To measure the noise of the multiplier, we use the scheme shown in Figure 3.16. The bandwidth limitation of the Phase Noise Analyzer requires the generation of an output signal with upper frequency of 400 MHz, i.e. an upper input frequency of 200 MHz. As before, to infer its behaviour in the final configuration at 400 MHz, we evaluate the dependence of the measured on the input frequency by repeating the measurement at 100 MHz and 200 MHz, generating respectively 200 and 400 MHz. The multiplier requires an input signal with power between 4 and 10 dBm. Considering the 6 dB input to output attenuation of the power splitter, the local oscillator is set to 16 dBm.

In both curves the measured noise level of the multiplier, especially in the region where flicker noise predominates, is limited by the noise floor of the Phase Noise Analyzer.

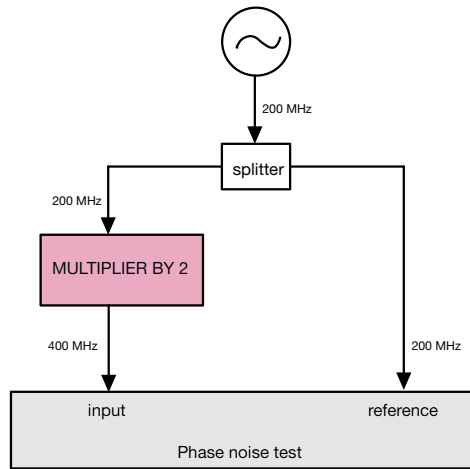


Figure 3.16: Configuration for multiplier by 2 phase noise measurement

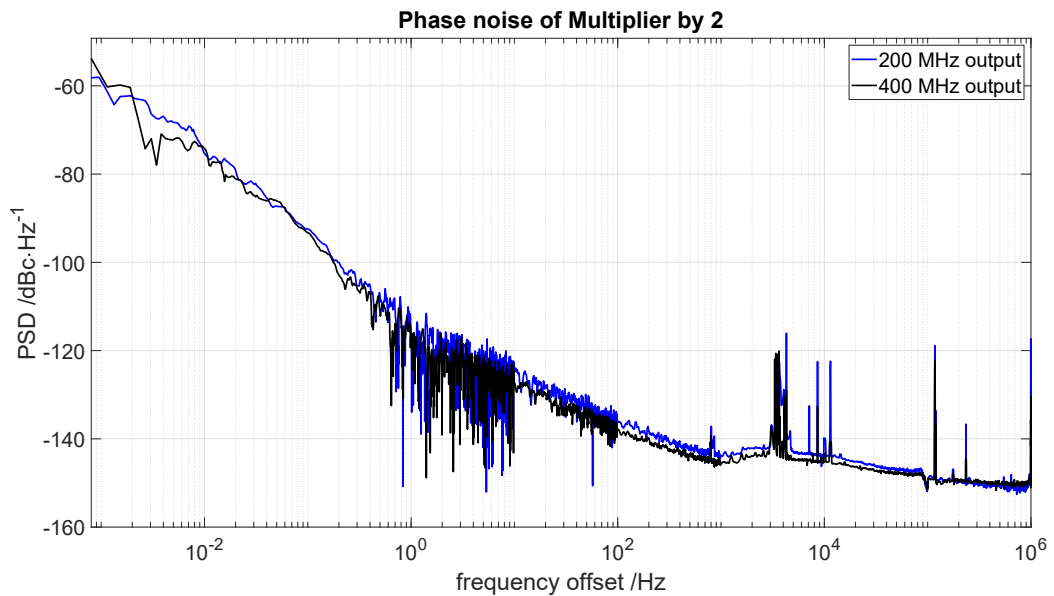


Figure 3.17: Phase noise of multiplier by 2 with 100 and 200 MHz input signals

The phase noise for both measurements is shown in Figure 3.17. The behaviour of the multiplier does not depend significantly on the input frequency: the discrepancy between the two curves is less than 1 dB and may be due to slightly different experimental conditions in the two measurements.

3.3.3 Noise of complete chain

The complete block diagram for measuring the phase noise of the second chain is shown in Figure 3.18.

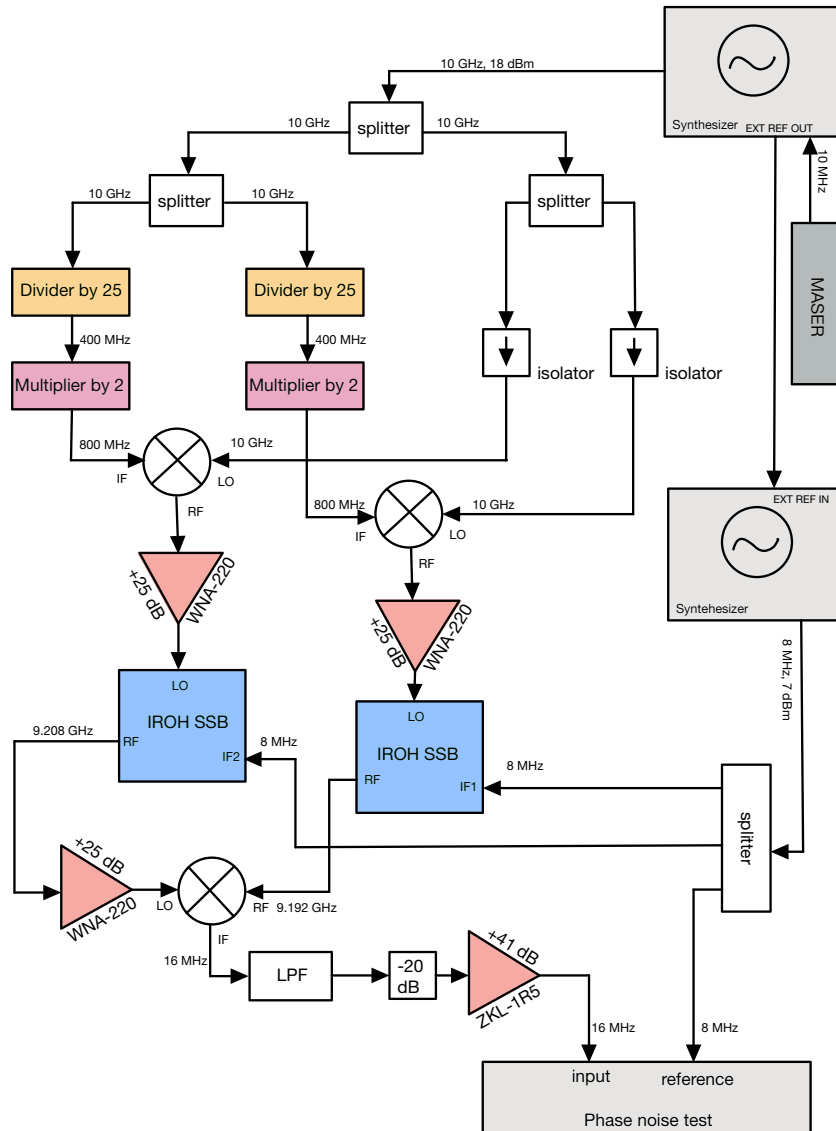


Figure 3.18: Complete second chain: from 10 GHz to 9.192 GHz

The first power splitter divides the 10 GHz input signal with power of 18 dBm: 6 dBm signal is sent to the left power splitter, 12 dBm to the right one. The two signals at 9.2

GHz are amplified by the WNA-220 amplifier to reach a sufficient level for the LO input of the single-sideband mixer. The IF ports are powered with a 8 MHz signal, 1 dBm, generated by a synthesizer with 7 dBm total power, split into three branches: two of them are sent to the two SSB mixers, the third is sent to the "reference" channel of the Phase Noise Analyzer.

The left SSB mixer generates a 9.208 GHz signal, the right one a 9.192 GHz signal. The 9.208 GHz signal is properly amplified using a WNA-220 amplifier sent to the LO input of the mixer together with the 9.192 GHz output of the other SSB mixer. The 16 MHz output of the mixer is sent to the "input" channel of the phase noise analyzer to be compared with the reference 8 MHz signal.

The phase noise of the second chain is shown in Figure 3.19.

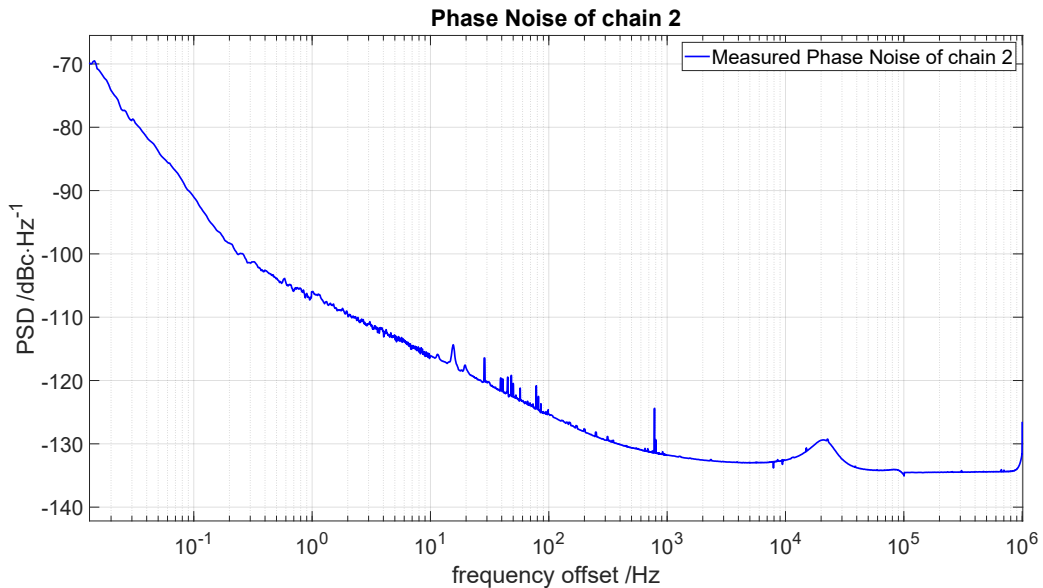


Figure 3.19: Phase noise of complete second chain: from 10 GHz to 9.192 GHz. 3 dB have been removed from the raw measurement to take into account that two identical chains were compared

The white noise level is about -134 dBc/Hz, while at 1 Hz, flicker noise at 1 Hz is about -106 dBc/Hz. The predominant contribution in white noise and in flicker noise is made by the noise of the divider by 25 properly scaled because the frequency of the signal generated by the divider is multiplied by a factor of 2 by the multiplier. The phase noise of the chain is consistent with the previously-calculated contributions of each component. This also means that the isolators, splitters and image-rejection mixer have a negligible influence on the determination of the noise budget of the chain.

Figure 3.20 and Figure 3.21 show the fundamental frequency 9.192 GHz with the harmonics generated by the entire chain with span equal to 200 kHz and 500 Hz respectively. It is possible to notice a 70 dB difference between the fundamental tone and the closest spur at 780 Hz. The rejection is even higher for other spurs. Overall, the performances of this chain are better than those of the first one.

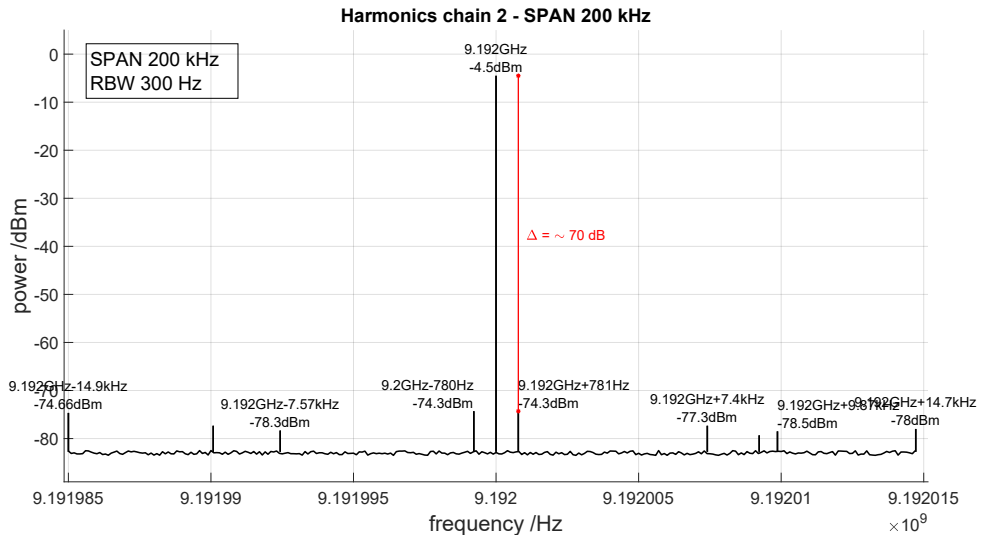


Figure 3.20: Harmonics of chain 2 with a SPAN of 200 kHz

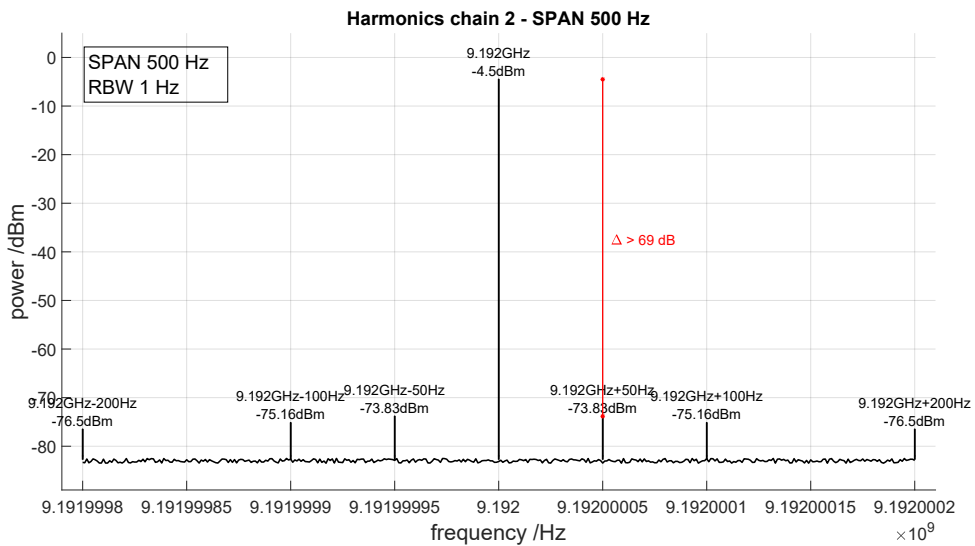


Figure 3.21: Harmonics of chain 2 with a SPAN of 500 Hz

3.4 Chains comparison

At this point, it is possible to summarize our results with a final comparison between the two chains. The phase noise curves obtained in the previous sections shown in Figure 3.11 and in Figure 3.19 are superimposed and shown in Figure 3.22 for an easier comparison and evaluation of the main differences.

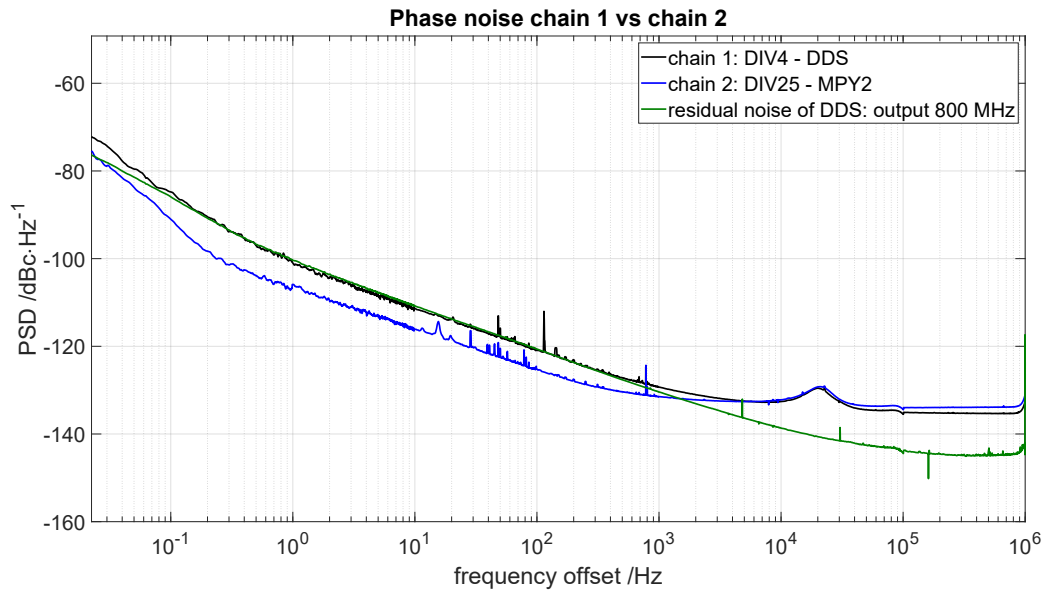


Figure 3.22: Comparison between phase noise of complete two chains and residual noise of the DDS. 3 dB have been removed from the measurement for each curve to take into account that two identical chains were compared

The white noise is similar for the two chains, -135 dBc/Hz for the first one and -134 dBc/Hz for the other; in both cases this is dominated by a combination of the white noise of the two amplifiers. A clear difference is instead observed on the flicker noise dominated region: at the frequency of 1 Hz the noise of the first chain is -101 dBc/Hz while for the second chain the noise at 1 Hz is 5 dB lower, -106 dBc/Hz. The predominant phase noise of the first chain is given by the DDS phase noise (green curve); the second chain does not integrate the DDS so the predominant phase noise in the flicker region is given by the noise of the divider by 25.

The second chain shows better performances also from the point of view of spurs. In sections 3.2.5 and 3.3.3 it was noticed that spur of the first chain at 50 Hz from the carrier had a power 62 dB lower than the main peak while the spur of the second chain at 50 Hz is 69 dB lower than the carrier. On the other hand, the other spurs were better suppressed in the second chain.

A further comparison is related to the curves obtained regarding the measurement of the Allan deviation of the two chains that enable to assess their long-term behaviour. The two curves relating to the Allan variance for the two chains are shown in Figure 3.23. The stability of the first chain is equal to $8 \cdot 10^{-16}$ at 1 s of averaging time, while the stability of the second chain is $3.4 \cdot 10^{-16}$.

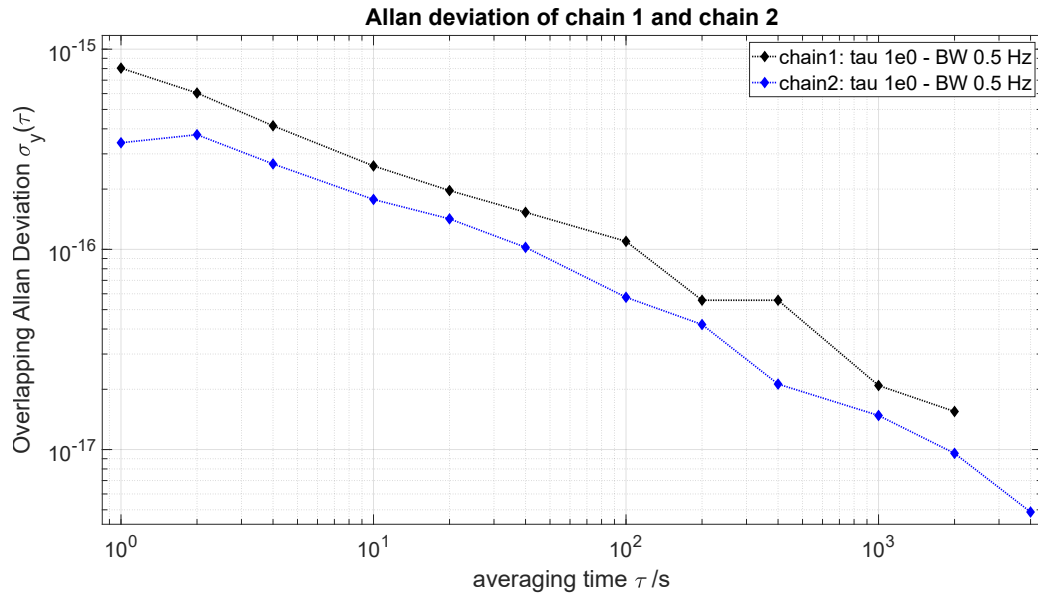


Figure 3.23: Comparison between Allan Deviation curves of two chains

Chapter 4

Analysis of long-term effects

Once the best chain was chosen for the reasons already expressed, the next step was to assess its long term behaviour, and in particular to characterize its temperature sensitivity.

4.1 Long-term measurement set-up

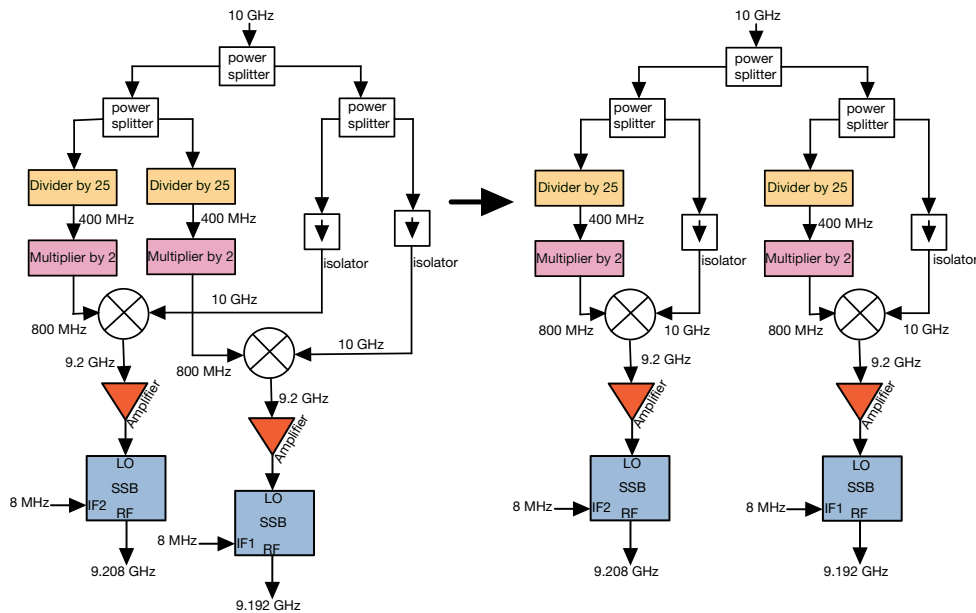


Figure 4.1: Block diagram of the chain as mounted for preliminar noise test (left), and in the present configuration (right)

The measurements reported in this session are again performed using two copies of the same chain. However, the detailed configuration is slightly changed as compared to the previous scheme. Figure 4.1 shows the old and new schemes.

On the left is represented the block diagram of the chain as mounted for preliminary noise test, also shown in Figure 3.18; on the right the present configuration is shown. In the left figure, after the first splitter, the chain is split into two branches, the one on the left generating two signals at 800 MHz, the one on the right distributing two signals at a frequency of 10 GHz; on the right configuration, the chains are re-organised to be independent: the first generates a signal at 9.192 GHz, the other the signal at 9.208 GHz. This change allowed to mount the two chains inside separate aluminum boxes to protect them from air currents and minimize the impact of environmental noise on the electronic paths; externally, the two outputs are mixed together to generate a 16 MHz signal.

A picture of the complete chain mounted inside the aluminum box is shown in Figure 4.2. The various signals and the names of the components used are indicated. The first signal on the right, named "IN: 10 GHz" is the signal entering the chain at a frequency of 10 GHz; the second signal from the right, named "IN: 8 MHz" is the 8 MHz signal used by the Single-Sideband Mixer to generate the 9.192 GHz signal. This is sent to the third connector from the right, named "OUT: 9.192 GHz". On the left side of the photo the power supply connectors are shown with red text: 12 V for the WNA-220 amplifier and 5 V to power the divider by 25 with a Common Ground.

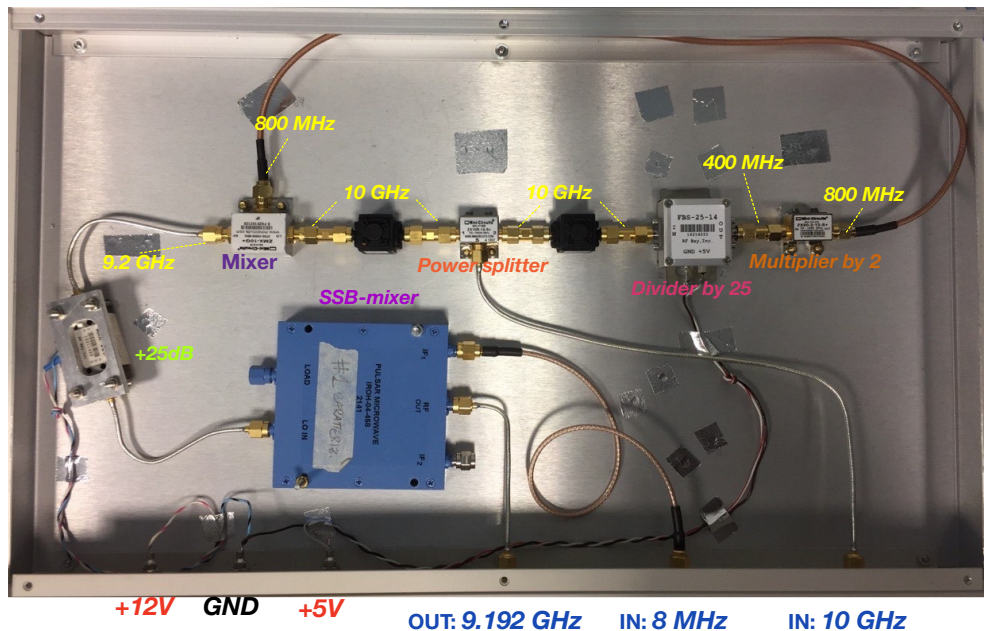


Figure 4.2: Chain 2 mounted inside the aluminum box.

4.2 Stability comparison between new and old chain

A long-term measurement is useful to measure the stability of the designed synthesis chain. Figure 4.3 shows the Allan Deviation of the designed chain compared with the Allan Deviation of the chain already functioning at INRiM. The stability of the old chain was measured following the same procedure as the current one.[12] The stability of the new chain is about 20 times better than the stability of the old chain.

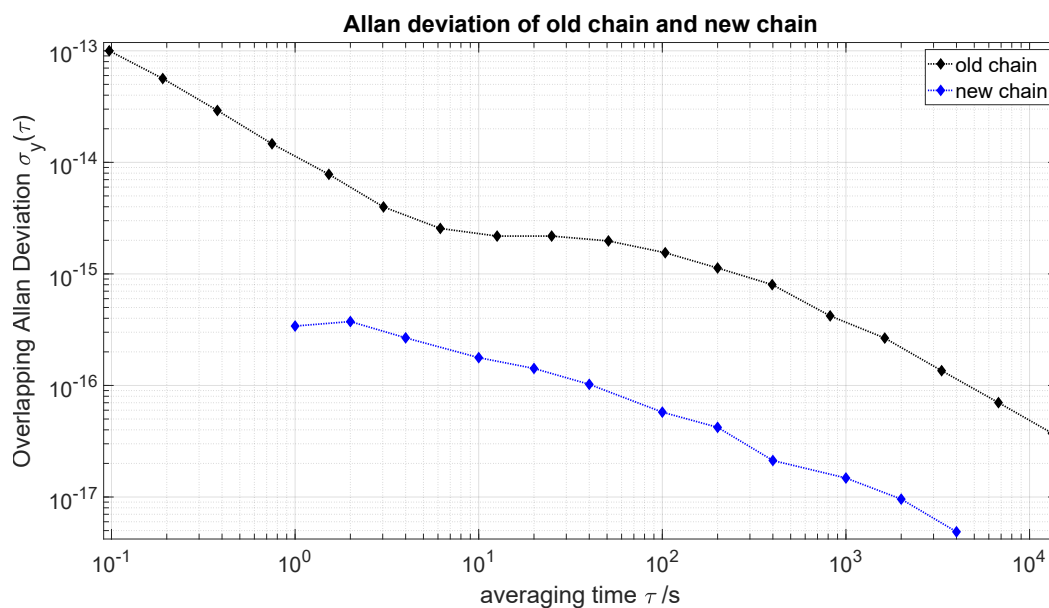


Figure 4.3: Frequency stability of previous chain vs new chain

4.3 Temperature sensitivity

In this section, the target is to characterize the temperature sensitivity of the synthesis chain. To obtain this value we induce temperature variation on the box containing the chain under test and record the corresponding phase shifts. The relationship between these two quantities provides the temperature sensitivity value in static conditions. The block diagram of the measurement is shown in Figure 4.4.

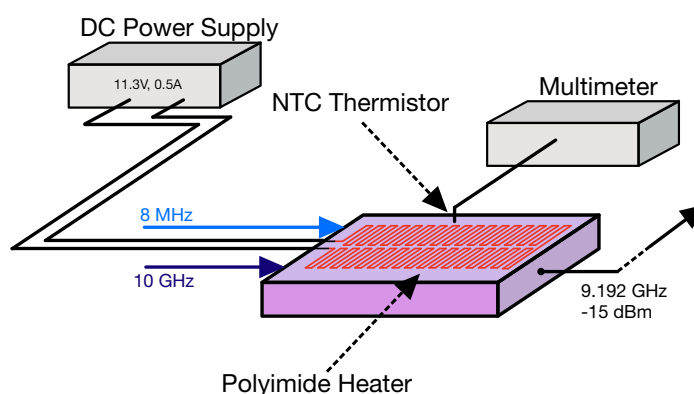


Figure 4.4: Measurement setup used to determine the temperature sensitivity

To measure the temperature, a Negative Temperature Coefficient (NTC) Thermistor with a temperature sensitivity of $400 \Omega/\text{C}$ and $10 \text{ k}\Omega$ resistance value at $25 \text{ }^\circ\text{C}$ is used. This sensor is mounted into the aluminum box, in thermal contact with the RF components; at the same time, the phase noise of the chain is measured by Phase Noise Analyzer.

A flexible Polyimide Heater, mounted in a Kapton foil, is applied using an adhesive on the upper surface of the aluminum box containing the chain under test that generates 9.192 GHz . The flexible heater is driven by a current generator with 11.3V and 0.5A setup, while the NTC Thermistor is connected to a multimeter which measures its resistance, from which the temperature is calculated.

Figure 4.5 shows two graphs: in the black curve the curve relating to the phase variation and in the blue curve the trend of the temperature inside the box indirectly computed from resistance measurement; the flexible heater was repeatedly switched on/off manually. The phase variation is highly correlated with the temperature inside the box. From the two curves it is possible to calculate the temperature sensitivity.

The phase variation is equal to $2.24 \cdot 10^{-3}$ cycles and the temperature variation ΔT is equal to 3.5 K . To express phase variation in radians it is necessary to multiply

the phase variation in cycles by 2π , $\Delta\phi|_{rad} = \Delta\phi|_{cycles} \cdot 2\pi = 14.1 \cdot 10^{-3}$ rad. The temperature sensitivity is calculated as $k = \Delta\phi|_{rad}/\Delta T|_K = 4 \cdot 10^{-3}$ rad/K. For easier comparison with results already published in the literature, the phase variation in radians is expressed in terms of time delay variations, following the mathematical expression $\Delta\phi|_s = \Delta\phi|_{rad}/(2\pi\nu|_{Hz}) = 2.44 \cdot 10^{-13}$ s where ν is the carrier frequency (9.192631770 GHz). The temperature sensitivity is $k|_{s/K} = \Delta\phi|_s/\Delta T|_K = 0.07$ ps/k.

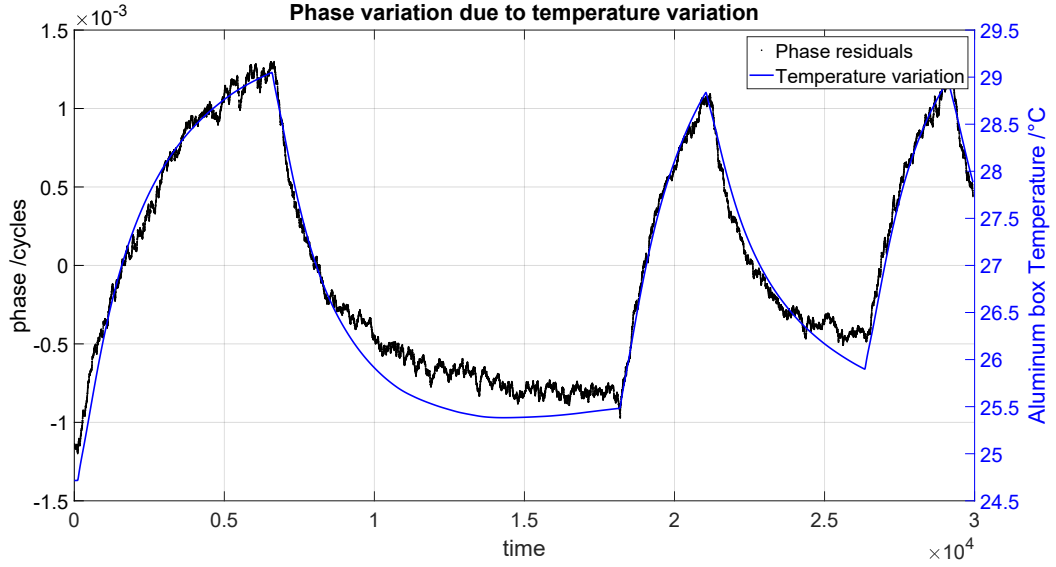


Figure 4.5: Temperature Sensitivity measurement

It is useful to compare it with other chains already built in other groups and whose results have been published. In [19] a temperature coefficient of 10 ps/K found, while in [20] the reported temperature coefficient is 1 ps/K. With a temperature sensitivity value equal to 0.07 ps/K, it is possible to conclude that the designed chain is less sensitive to temperature compared to similar chains.

Once the temperature sensitivity coefficient has been obtained, another aspect should be considered. The laboratory is a thermostated environment, and assuming that the air conditioner introduces a periodical disturbance at 1000 s it is necessary to evaluate how the ventilation system affects the stability measurement. We suppose the room temperature can be described by a periodical function of the form

$$T(t) = T_0 + \Delta T \sin(2\pi \cdot f_T t) \quad (4.1)$$

where $T_0 = 25^\circ\text{C}$ is the average temperature, ΔT in the range 0.1°C to 1°C is the typical temperature excursion, and $f_T = 10^{-3} \text{ s}^{-1}$ is the frequency of air conditioning cycle.

The phase ϕ is highly correlated with temperature, and can be expressed as:

$$\phi(t) = \phi_0 + \Delta\phi \sin(2\pi \cdot f_T t) \quad (4.2)$$

where ϕ_0 is a constant, arbitrary phase. The amplitude of the periodical phase variations can be expressed as $\Delta\phi = k \cdot \Delta T$ where $k = 4 \cdot 10^{-3}$ rad/K, is the the temperature sensitivity derived from the procedure described above. Because the instantaneous frequency of an oscillator can be expressed as

$$\Delta\nu(t) = \frac{1}{2\pi} \frac{d\phi(t)}{dt} \quad (4.3)$$

it is easy to see that any change in the phase introduced by the chain will also affect the frequency of the signal passing through it. The relative frequency variations can be written in relative terms as:

$$\frac{\Delta\nu_0}{\nu_0} = \frac{1}{2\pi \cdot \nu_0} \frac{d}{dt} [\phi_0 + k\Delta T \cdot \sin(2\pi \cdot f_T t)] = \frac{k\Delta T}{2\pi \cdot \nu_0} 2\pi \cdot f_T \cdot [\cos(2\pi \cdot f_T t)] = \frac{k\Delta T}{\nu_0} f_T \quad (4.4)$$

Assuming a 1°C of temperature excursion, $\nu_0 = 9.192631770$ GHz and $f_T = 10^{-3} s^{-1}$, the expected peak-to-peak relative fluctuations of the generated microwave due to a temperature changes of the laboratory would be $\Delta\nu/\nu_0 = 4.35 \cdot 10^{-16}$.

It is thus important that the chain is subject to maximum temperature excursions of 0.1°C in order to ensure that the frequency instability due to the temperature is negligible compared to the typical instability of the fountain, i.e. $< 10^{-16}$.

We measured the typical temperature variations inside the box when it is placed in the fountain clock laboratory. The data collection is reported in Figure 4.6. It is possible to notice a temperature variation from 24.05°C to 24.15°C, a $\Delta T=0.1$ K on the long term, with about 20 mK periodical oscillations due to the air conditioning system.

Assuming these temperature fluctuations affect the phase with the previously determined sensitivity coefficient $k=0.07$ ps/K, we can derive the corresponding frequency fluctuations using Equation 4.3 and the expected Allan deviation. This is shown in Fig.4.7.

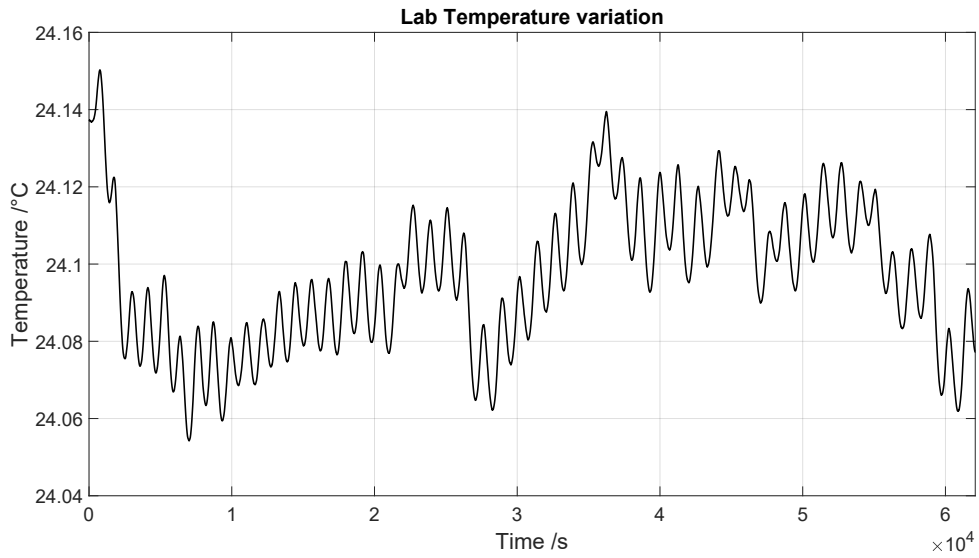


Figure 4.6: Temperature variation in the Measurement Lab

The curve shows a bump at an observation time of about 500 s, which indicates the introduction of a disturbance at 1000 s. Despite the bump, if we compare the curve obtained with the curve of the Allan deviation of the designed chain reported in Figure 4.3, it is possible to conclude that the variations in temperature have a negligible effect on the chain.

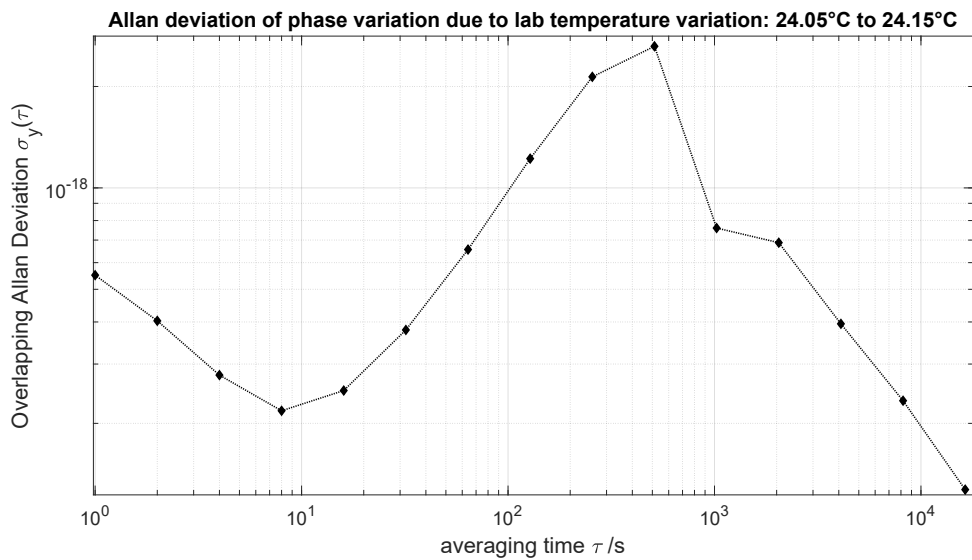


Figure 4.7: Allan Deviation curve of Temperature variation in the Measurement Lab

Chapter 5

Stability measurements with the new synthesis chain

In this last chapter, the basic idea is to demonstrate the correct functioning of the complete system composed of the laser, the optical comb, and the chain to interrogate the atoms of the fountain. First, the chain is seeded by a 10 GHz signal produced by the microwave synthesis module of the optical comb; in turn, the comb is phase-locked to an ultra-stable laser with typical stability of $2 \cdot 10^{-15}$. We will confirm the absence of spurs in the final configuration by repeating the measurement on the RF spectrum analyzer. Finally, in the second part of the chapter, the optically-synthesized microwave with superior spectral purity is used in the fountain to interrogate Cs atoms, to assess improvements in instability thanks to a possible reduction of the Dick effect.

5.1 Microwave synthesis with the Optical Comb

The optical signal at 10 GHz generated by the Comb is converted into the microwave at 10 GHz which will be sent to the input of the synthesis chain.

The module is integrated into the setup shown in Figure 5.1 and connected to the synthesis chain. The Optical Comb's output optical power is 14 dBm. According to specifications, the photodiode accepts a maximum power of 5 mW: the Optical Comb signal is attenuated by means of a 15 dB optical attenuator. The 10 GHz Menlo System output signal is a power of 15 dBm, since the synthesis chain requires an input power level equal to 12 dBm, a 3 dB attenuator is added at the 10 GHz input channel. An 8 MHz signal with a power of 7 dBm is generated by a waveform generator and sent to the IF input of the image-rejection mixer.

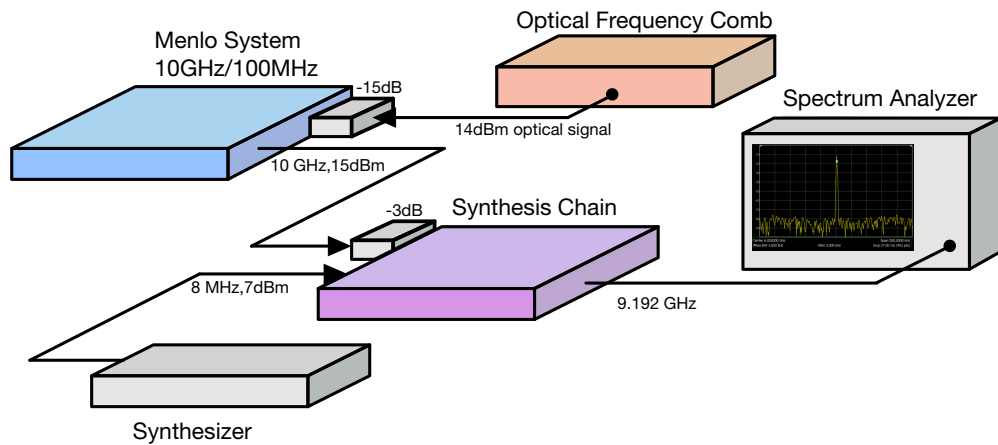


Figure 5.1: Measurement scheme with Optical Frequency Comb

The output of the chain is then sent to the spectrum analyzer to assess the presence of spurs, and the corresponding spectrum. The spectrum is shown in Figure 5.2 with a SPAN of 400 MHz. The signal generated by the synthesis chain at 9.192 GHz has a power of about -8 dBm.

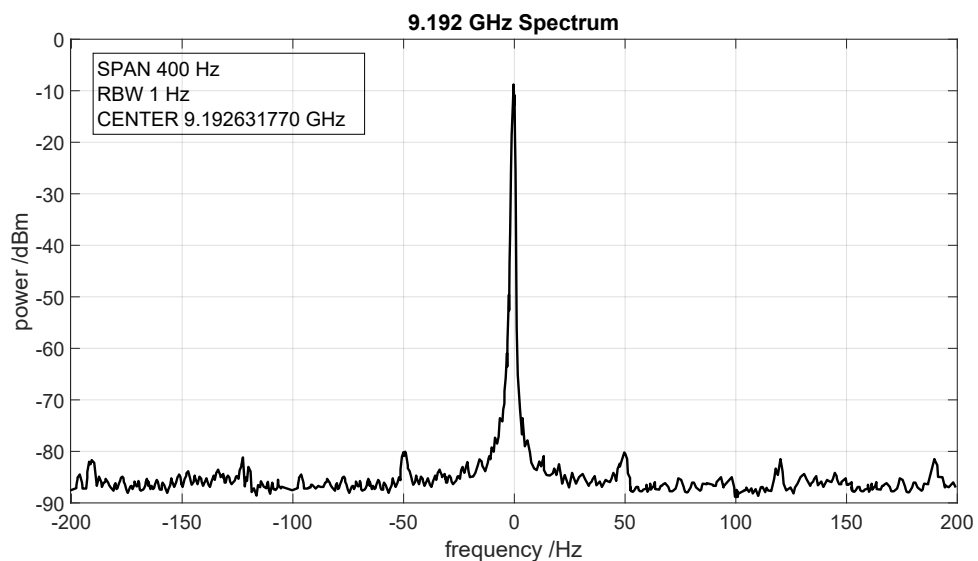


Figure 5.2: Spectrum of complete chain with Optical Comb signal as input

The spurs are quite symmetrical and those of greatest influence are at 50 Hz, 120 Hz, and 190 Hz away from the 9.192 GHz signal. At 50 Hz the spurious is about -80 dBm,

72 dB lower than the carrier, at +120 Hz the spurious is about -81 dBm, 73 dB lower than the carrier and at +190 Hz, with about -82 dBm, the spurious is about 74 dB lower with respect the carrier. From the reported results, we conclude that also in the final configuration the spectral purity of the chain is suitable for atoms interrogation, as no systematic shifts on the fountain clock are expected with the measures level of spurs.

The phase noises of the elements of the system: the laser, the unit module, and the synthesis chain are shown in Figure 5.3. The ultra-stable laser spectrum is scaled from 5000 THz to 10 GHz and compared with the specified phase noise of the microwave unit (Menlo module) and the phase noise of the designed chain.

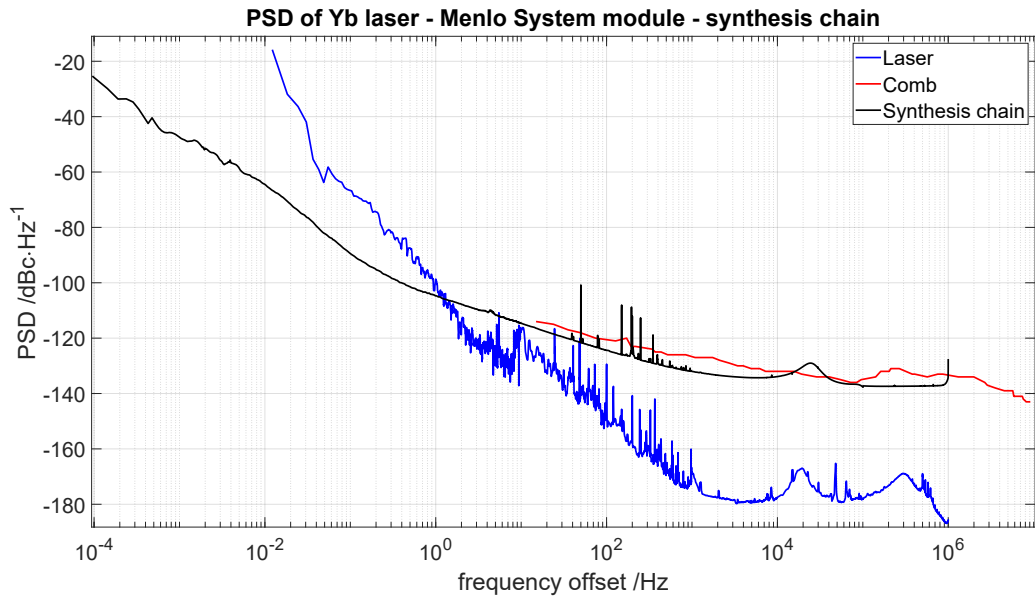


Figure 5.3: PSD of Yb laser, Comb and the conversion unit and synthesis chain

As can be seen from Figure 5.3 the noise of the microwave that interrogates the fountain is dominated, in the range 1 – 10 Hz, by the noise of the synthesis chain and by the Comb. In this case, it can be seen how the phase noise of the synthesis chain is lower than the noise of the Comb. If the first chain had been chosen rather than the second, the overall contributed noise would have been larger.

5.2 Interrogating Cs atoms in the fountain clock with the optically-synthesized microwave

The chain generates a signal at a frequency equal to the difference between 9.2 GHz and the frequency of an external DDS. The DDS frequency represents an adjustable frequency correction that allows fine-tuning the microwave signal to constantly keep it on resonance with Cs atoms.

5.2.1 Ramsey scans

Figure 5.4 shows the so-called Ramsey scan. The differences between the atomic resonance of the fountain and the frequency of the microwave sent to the fountain are shown on the horizontal axis; on the vertical axis, on the other hand, the probability of having atoms is reported as a function of the above-mentioned differences. From the Figure, it is, therefore, possible to notice that the maximum probability reached is at an offset of +0.6 Hz. Ramsey's spectroscopy in conclusion shows if the microwave frequency is centered on the atomic resonance of the fountain.[15]

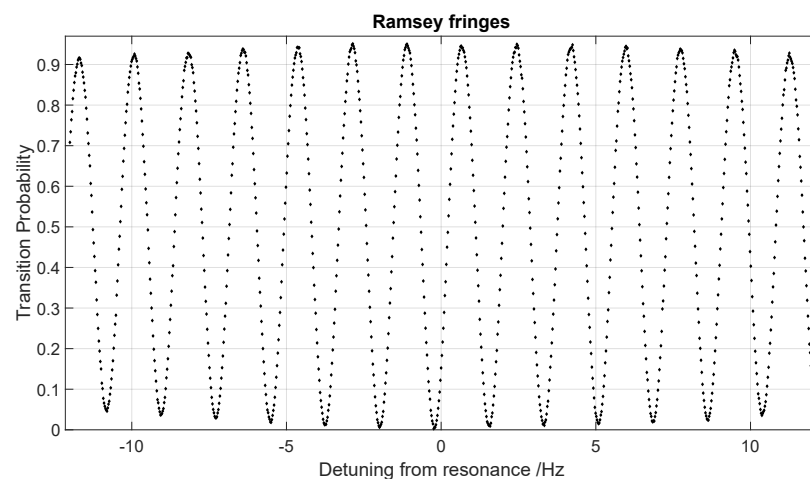


Figure 5.4: Ramsey fringes

5.2.2 Stability measurement

To obtain information on relative stability of the Cs fountain lock it is necessary to consider the data collected on the DDS correction frequency. The most significant comparison between the two chains is thus obtained by comparing the fountain clock stability achieved with the two chains. The results are shown in Figure 5.5.

The expected stability curves calculated knowing that the stability of the Cs clock should decrease inversely proportional to $\sqrt{\tau}$, where τ is the measurement time, are shown in ocher and magenta.

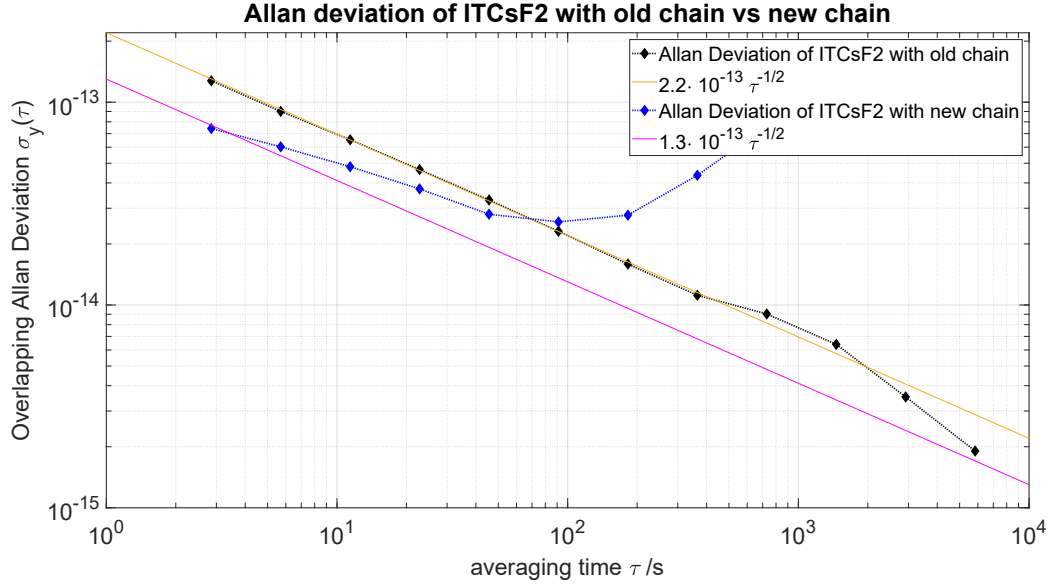


Figure 5.5: Frequency stability of fountain with old chain vs new chain

At 1 s the stability of the designed chain is $1.3 \cdot 10^{-13}$, while the stability of the old chain is $2.2 \cdot 10^{-13}$, i.e. a factor of 2 improvement is observed. At averaging times longer than 1s, the long-term instability of the ultra-stable laser emerges. During the clock operation, this long-term instability will be further suppressed by external locking method for the ultra-stable laser. In terms of averaging time, this means that only 18 days are needed to achieve an ultimate instability of 10^{-16} , instead of 72 days as with the present chain. This represents a factor of 4 improvement.

The design of the chain and therefore of the system represents an element of considerable importance for the frequency measurements of the optical standards present at INRiM, currently limited by the stability of the primary standard.

Conclusion

The objective of my thesis was the design and realization of a low-noise microwave synthesis chain to interrogate Cs atoms in an atomic clock with improved instability than the existing one. This objective was achieved, as the obtained instability was reduced by a factor of 2. This improvement is obtained thanks to the reduction of the Dick effect, originated from the synthesis chain noise in spectral range 1 – 10 Hz. In terms of averaging time, this means that only 18 days are needed to achieve an ultimate instability of 10^{-16} , instead of 72 days as with the present chain. This represents a factor of 4 improvement.

In the frequency range between 1 Hz and 10 Hz the realized chain has a phase noise lower than the optical frequency comb, below which it is not possible to improve the system. In addition, it has been shown that the new chain suffers less from the presence of spurious signals than the previous one: their level is about -70 dBc at 50 Hz. This is relevant in view of its use in the atoms interrogation, where the presence of spurs might affect the spectroscopic measurement.

A further improvement was obtained regarding temperature sensitivity with a value of 0.07 ps/K compared to 1 ps/K of the chain present at INRiM.

In the forthcoming weeks, an atomic clock measurement campaign is planned using the new chain. Through these measurements the ultimate performances will be measured and will allow to insert the chain in the measurement system.

The path to follow for the redefinition of the second has already been undertaken and soon the Caesium will be replaced, however, using the realized chain it will be possible to perform faster measurements of Caesium and also of Caesium compared to optical clocks.

Datasheet

 **5120 Microsemi Phase Noise Analyzer:**

title: "5125A High-Performance Phase Noise, Extended-Range Phase Noise and Allan Deviation Test"

url: <https://www.microsemi.com/product-directory/phase-noise-and-allen-deviation-testers/4129+5125aresources>;

 **Divider by 4:**

title: "HMC365G8 - SMT GaAs HBT MMIC - DIVIDE-BY-4 - DC - 13 GHz"

url: <https://www.analog.com/media/en/technical-documentation/data-sheets/hmc365g8.pdf>;

 **DDS - Direct Digital Synthesizer:**

title: "AD9914 - 3.5 GSPS Direct Digital Synthesizer with 12-Bit DAC"

url: <https://www.analog.com/media/en/technical-documentation/data-sheets/AD9914.pdf>;

 **Divider by 25:**

title: "FBS-N-14 - 100MHz–14GHz Divide-By-N Prescaler"

url: https://rfbayinc.com/products_pdf/product_2_273.pdf;

 **Multiplier by 2:**

title: "ZX90-2-13-S+ - x2 Frequency Multiplier - 50 Ω Output - 20 to 1000 MHz"

url: <https://www.minicircuits.com/pdfs/ZX90-2-13-S+.pdf>;

 **High frequency Amplifier:**

title: "WNA-220 - 10MHz–10GHz Low Noise Amplifier"

url: https://rfbayinc.com/products_pdf/product_1_689.pdf;

 **Low frequency Amplifier:**

title: "ZKL-1R5+ - Coaxial Amplifier - 50 Ω Medium Power - 10 to 1500 MHz "

url: <https://www.minicircuits.com/pdfs/ZKL-1R5+.pdf>;

 **Single Sideband Mixer:**

title: "IROH-04-458 - IMAGE REJECT MIXER"

url: https://www.pulsarmicrowave.com/spec_sheets/IROH-04-458.pdf;

 **High Frequency Mixer:**

title: "ZMX-10G+-ZMX-10G - Coaxial Frequency Mixer - Level 7 (LO Power +7 dBm) - 3700 to 10000 MHz"

url: <https://www.minicircuits.com/pdfs/ZMX-10G.pdf>;

 **Power splitter 1 to 2:**

title: "ZX10R-14-S+ - 2 Way-0° Resistive 50 Ω - DC to 10000 MHz - Coaxial Power Splitter/Combiner"

url: <https://www.minicircuits.com/pdfs/ZX10R-14-S+.pdf>;

 **Power splitter 1 to 3:**

title: "ZCSC-3-R3+ - 3 Way-0° 50 Ω - 2 to 300 MHz - Coaxial Power Splitter/Combiner"

url: <https://www.minicircuits.com/pdfs/ZCSC-3-R3+.pdf>.

Bibliography

- [1] SAFE LOAD testing technologies. *PSD definition*. URL: <https://www.safeloadtesting.com/power-spectral-density/> (cit. on p. 3).
- [2] E.Rubiola. «Almost All About Phase Noise». In: *Microwave and Wireless Synthesizers*, 2nd ed., Wiley 2020 () (cit. on pp. 3–7).
- [3] Rubiola-Calosso. *A Tutorial on Phase Noise*. URL: https://indico.fnal.gov/event/21836/contributions/64988/attachments/40841/49444/Enrico_LLRF-2019-Tutorial.pdf (cit. on p. 5).
- [4] Microsemi. *5125 - High-Performance, Extended-Range Phase Noise and Allan Deviation Test Set* (cit. on p. 7).
- [5] *Phase Noise Test Set (5120A / 5120A-01 / 5115A) Operations and Maintenance Manual*. Symmetricon. 2009 (cit. on p. 8).
- [6] Wikipedia. *Covarianza (probabilità)*. URL: [https://it.wikipedia.org/wiki/Covarianza_\(probabilit%C3%A0\)](https://it.wikipedia.org/wiki/Covarianza_(probabilit%C3%A0)) (cit. on p. 9).
- [7] Chiara Moreschini. *Riassunti di Fondamenti di Segnali per Ingegneria Biomedica*. URL: https://www.andreadd.it/appunti/polimi/ingegneria/corsi/ing_biomedica/Anno2/statistica_segnali_biomedici/appunti/Riassunto_segnali_biomedici1819new.pdf (cit. on p. 9).
- [8] *Allan Variance*. URL: <https://home.engineering.iastate.edu/~shermanp/AERE432/lectures/Rate%5C%20Gyros/Allan%20variance.pdf> (cit. on p. 9).
- [9] *Definizione di Secondo*. URL: <https://www.chimica-online.it/download/definizione-di-secondo.htm> (cit. on p. 11).
- [10] Filippo Bregolin. *171Yb optical frequency standards towards the redefinition of the second* (cit. on pp. 11, 12).
- [11] Heavner Parker Shirley Kunz Jefferts. *NIST F1 AND F2*. URL: <https://tf.nist.gov/general/pdf/2500.pdf> (cit. on p. 12).

- [12] Levi-Calonico-Calosso-Godone-Micalizio-Costanzo. *Accuracy evaluation of ITCsF2, a Nitrogen cooled Cesium Fountain* (cit. on pp. 12, 15, 44).
- [13] R.Wynands and S.Weyers. «Atomic Fountain Clock». In: *Metrologia*, vol.42, numb.3 - BIPM and IOP Publishing Ltd (2005) (cit. on p. 13).
- [14] l'Observatoire de Paris - PSL Syrte. *The atomic fountains - Principle of operation*. URL: <https://synte.obspm.fr/spip/science/references-micro-ondes-et-echelles-de-temps/activites-138/horloges-a-fontaines-atomiques/article/principe-of-operation?lang=en> (cit. on p. 14).
- [15] Wikipedia. *Ramsey interferometry*. URL: https://en.wikipedia.org/wiki/Ramsey_interferometry (cit. on pp. 14, 53).
- [16] Tara Fortier and Esther Baumann. «20 years of developments in optical frequency comb technology and applications». In: *Communications PHYSICS* () (cit. on pp. 16, 17).
- [17] Menlo System GmbH. *Test Report* (cit. on p. 18).
- [18] Wikipedia. *Direct Digital Synthesis*. URL: https://en.wikipedia.org/wiki/Direct_digital_synthesis (cit. on p. 20).
- [19] Heavner-Jefferts-Donley-Parker-Levi. *A New Microwave Synthesis Chain for the Primary Frequency Standard NIST-F1* (cit. on p. 46).
- [20] Kazda-Gerginov-Lipphardt-Weyers. *Microwave Synthesis for the PTB Cesium Fountain Clocks* (cit. on p. 46).

